



HAL
open science

Seismic and aseismic slip during the 2006 Copiapó swarm in North-Central Chile

Javier Ojeda, Catalina Morales-Yáñez, Gabriel Ducret, Sergio Ruiz, Raphael Grandin, Marie-Pierre Doin, Christophe Vigny, Jean-Mathieu Nocquet

► **To cite this version:**

Javier Ojeda, Catalina Morales-Yáñez, Gabriel Ducret, Sergio Ruiz, Raphael Grandin, et al.. Seismic and aseismic slip during the 2006 Copiapó swarm in North-Central Chile. *Journal of South American Earth Sciences*, 2023, 123, pp.104198. 10.1016/j.jsames.2023.104198 . hal-03990770

HAL Id: hal-03990770

<https://hal.science/hal-03990770>

Submitted on 18 Jan 2024

HAL is a multi-disciplinary open access archive for the deposit and dissemination of scientific research documents, whether they are published or not. The documents may come from teaching and research institutions in France or abroad, or from public or private research centers.

L'archive ouverte pluridisciplinaire **HAL**, est destinée au dépôt et à la diffusion de documents scientifiques de niveau recherche, publiés ou non, émanant des établissements d'enseignement et de recherche français ou étrangers, des laboratoires publics ou privés.

1 Highlights

2 **Seismic and aseismic slip during the 2006 Copiapó swarm in North-Central Chile**

3 Javier Ojeda, Catalina Morales-Yáñez, Gabriel Ducret, Sergio Ruiz, Raphael Grandin, Marie-Pierre Doin, Christophe
4 Vigny, Jean-Mathieu Nocquet

- 5 • We provide a seismological and geodetic analysis of a three-week-long seismic swarm that occurred at the North-
6 Central Chile subduction zone in 2006.
- 7 • Seismological analysis reveals a complex seismicity migration pattern involving two $M \sim 6.5$ -6.6 earthquakes.
- 8 • Geodetic data suggest that slow aseismic slip occurs at the beginning of the sequence and then afterslip down-dip
9 of the two largest earthquakes.
- 10 • The observed diversity of slow and fast slip likely results from the subduction of Copiapó Ridge seamounts.

Seismic and aseismic slip during the 2006 Copiapó swarm in North-Central Chile

Javier Ojeda^{a,b,c,*}, Catalina Morales-Yáñez^d, Gabriel Ducret^e, Sergio Ruiz^b, Raphael Grandin^a, Marie-Pierre Doin^f, Christophe Vigny^g and Jean-Mathieu Nocquet^{h,a}

^aUniversité Paris Cité, Institut de Physique du Globe de Paris, CNRS, Paris, France

^bDepartamento de Geofísica, Universidad de Chile, Santiago, Chile

^cDepartamento de Geología, Universidad de Chile, Santiago, Chile

^dDepartamento de Ingeniería Civil, Universidad Católica de la Santísima Concepción, Concepción, Chile

^eInstitut Français du Pétrole Energies Nouvelles, Reuil-Malmaison, France

^fUniversité Grenoble Alpes, Université Savoie Mont Blanc, CNRS, IRD, Université Gustave-Eiffel, ISTERre, Grenoble, France

^gLaboratoire de Géologie - CNRS UMR 8538, École Normale Supérieure - PSL University, Paris, France

^hUniversité Côte d'Azur, Géoazur, IRD, CNRS, Observatoire de la Côte d'Azur, Valbonne, France

ARTICLE INFO

Keywords:

Seismic swarm

Short term slow slip event

Aseismic deformation

Subduction zone processes

Copiapó

Chile

ABSTRACT

Earthquake swarms commonly occur along the Chilean subduction zone, witnessing fast seismic and slow aseismic slip behavior at the plate interface. However, the largest seismic swarms observed in Chile, particularly in the Copiapó-Atacama region, remain poorly documented, and the underlying processes have yet to be understood. Here, we perform seismological and geodetic analyses to investigate the 2006 Copiapó swarm, which developed in April and May 2006. The swarm began on April 19, with a magnitude M_L 5.3 earthquake. During the nine following days, we observe a migration of seismicity along the plate interface, the occurrence of doublets events, and a potential slow slip event in the GPS time series at site Copiapó. Then, on April 30, a first earthquake with M_w 6.6 occurred at 15 km depth at the plate contact. It likely triggered a second earthquake of magnitude M_w 6.5, which occurred 144 minutes later, 10 km northwest of the first earthquake. Using InSAR, we determined the slip distribution and moment release associated with these two earthquakes and detailed the “postseismic” slip they triggered in the next days and weeks. This postseismic phase appears to be predominantly aseismic, while the moment released during the “coseismic” phase is comparable to other seismic crises that occurred in Atacama. Although we did not find a larger seismic and aseismic ratio than in other swarms in South America, we suggest a similar mechanism of slow deformation as a driver of seismicity during seismic swarms. Finally, we propose that the slow and fast behavior of the 2006 Copiapó swarm is a consequence of the subduction of the Copiapó Ridge seamounts, which affects both the plate interface and the overriding plate by inducing complex interactions between seismic and aseismic processes.

*Corresponding author

ojeda@ipgp.fr (J. Ojeda); catalina.morales@ucsc.cl (C. Morales-Yáñez); gabriel.ducret@ifpen.fr (G. Ducret); sruiz@uchile.cl (S. Ruiz); grandin@ipgp.fr (R. Grandin); marie-pierre.doin@univ-grenoble-alpes.fr (M. Doin); vigny@biotite.ens.fr (C. Vigny); nocquet@geoazur.unice.fr (J. Nocquet)

ORCID(s): 0000-0002-7188-8356 (J. Ojeda); 0000-0002-3230-1014 (C. Morales-Yáñez); 0000-0001-7511-2910 (G. Ducret);

48 **1. Introduction**

49 The North-Central Chile subduction zone is characterized by significant background seismicity, the occurrence of
50 large earthquakes, and episodic seismic swarms that reflect the wide variability of slip behavior in this tectonic setting.
51 Previous studies propose that the bathymetric heterogeneities along the subducting plate, such as fracture zones or
52 oceanic ridges, could explain the diversity of the slip modes and also the along strike segmentation in subduction zones
53 (e.g., [Poli et al., 2017](#); [Maksymowicz, 2015](#); [Pastén-Araya et al., 2022](#)). Indeed, oceanic features such as fracture zones
54 have been related to the presence of hydrated sediments and fluids (e.g. [Peacock, 1990](#); [Manea et al., 2014](#); [Nishikawa
55 and Ide, 2015](#)). Seamounts and oceanic ridges impact the dynamics of subduction zones ([Morell, 2016](#)) defining
56 potential barriers to large seismic ruptures (e.g. [Contreras-Reyes and Carrizo, 2011](#); [Das and Watts, 2009](#)). These
57 interpretations led to correlate the presence of these subducted oceanic features with high pore pressure content inside
58 a fluid-rich system that may drive the observed diversity of slip modes and, more especially, those related to seismic
59 swarm activity ([Nishikawa and Ide, 2017](#)).

60 The Copiapó-Atacama area hosted large earthquakes (Fig. 1). Archaeological and paleoseismological inferences
61 from [Salazar et al. \(2022\)](#) allowed them to identify a mega-earthquake that occurred ~3800 yrs ago, which may explain
62 the awareness and lifestyle changes of the inhabitants along the coastal area of northern Chile. Besides, the 1420 Oei
63 orphan tsunami could possibly be attributed to a great earthquake magnitude $M_{8.8-9.4}$ ([Abad et al., 2020](#)) along the
64 Atacama segment. Other large earthquakes occurred in 1819 (M_s 8.3) and 1922 (M_w 8.5-8.6) ([Beck et al., 1998](#);
65 [Kanamori et al., 2019](#); [Carvajal et al., 2017](#)), while several earthquakes magnitude $M \sim 7$ or similar have been reported
66 in 1796, 1859, 1909, 1918, 1946, and 1983 ([Comte et al., 2002](#); [Ruiz and Madariaga, 2018](#)). Recent studies have
67 shown that the Atacama segment experiences both seismic and aseismic slips. [Klein et al. \(2018a\)](#) detected a slow slip
0000-0003-1758-0788 (S. Ruiz); 0000-0002-1837-011X (R. Grandin); 0000-0002-9546-4005 (M. Doin); 0000-0002-3436-9354 (J.
Nocquet)

68 event (SSE) between 2014 and 2016 below the city of Copiapó, representing the first deep long-term SSE documented
69 in Chile. The deep SSE is located in a low coupled zone (Klein et al., 2018b; Métois et al., 2014), and exhibits a
70 potential recurrent pattern of about 4-5 years since the same transient signal was recorded by a continuous GPS station
71 in 2005, 2009, 2014 and more recently in 2020 (Klein et al., 2022a). Interestingly, seismic and aseismic signatures
72 have also been observed through the seismicity distribution, non-volcanic tremors, and repeaters events (Pastén-Araya
73 et al., 2022). Those signals are placed in areas of V_p , V_s , and V_p/V_s ratio anomalies, pointing out the subduction
74 of the Copiapó Ridge as an important bathymetric feature controlling the along-strike and along-dip changes of slip
75 behaviors. The Copiapó Ridge, built by hotspot tracks in the Nazca plate, is characterized by a rough and discontinuous
76 topography that formed its seamounts. This oceanic feature had different migration episodes in the last 60 Ma that
77 coincides with the southward migration of the flat slab, suggesting a key role of oceanic ridges such as Copiapó, Juan
78 Fernández, or Tal Tal in the deformation process along North-Central Chile (Bello-González et al., 2018).

79 Over the last 50 years, repeated occurrences of seismic sequences and seismic swarms have been observed in the
80 Atacama region (see Fig. S1). For instance, the sequences occurring at latitudes 27.5°S - 28°S in 2002, 2011, and
81 more recently during 2020 in Vallenar-Atacama (Klein et al., 2021) or the swarm episodes of 1973, 1979, 2006 (Comte
82 et al., 2002; Holtkamp et al., 2011), and 2015 offshore the cities of Caldera and Copiapó at latitudes 26.7°S - 27.5°S
83 (Fig. 1, see Fig. S1). Precisely in Copiapó, one of the most productive seismic swarms that have been observed
84 in Chile and South America occurred between April and May 2006. The Copiapó area is characterized by low V_p
85 and high V_p/V_s (Comte et al., 2006), indicating the presence of fluid-richness, spatially correlated with the location
86 of a subducting seamount. Furthermore, Holtkamp et al. (2011) used the NEIC seismic catalog and InSAR imagery
87 to analyze the 2006 seismic swarm, estimating a seismicity migration of about ~ 7 km/day during the sequence, but
88 also suggesting that the observed ground deformation could not require an important contribution of aseismic slip.

89 However, it remains unclear how the Copiapó swarm evolved spatiotemporally and whether the scarce seismological
90 local data and geodetic observations can reveal any component of aseismic slip.

91 In this study, we revisit the fast and slow processes during the 2006 swarm (Fig. 2) that occurred offshore the
92 cities of Copiapó and Caldera in the Atacama region, North-Central Chile. The seismic swarm initiated on April
93 19, with an earthquake magnitude M_l 5.3 accompanied by doublet earthquakes and a slight westward transient in the
94 single GPS station available in the area. After a few days of lower intensity in the seismic activity, the two largest
95 earthquakes magnitude $M_w \sim 6.5$ -6.6 occurred on April 30, separated by 2.4 hours. We used the available geodetic and
96 seismological data to understand the slip behavior that drove this swarm. Our analysis shows that the Copiapó swarm
97 produced complex interactions along the plate interface, which may be accompanied by a possible short-term SSE.
98 The swarm is spatially correlated with a subducted oceanic seamount, possibly responsible for the seismicity pattern
99 through time.

100 2. Data and Methods

101 2.1. Regional seismic data and processing

102 To perform our seismological analysis, we used regional short-period, three-component seismic stations deployed
103 by the National Seismological Service of the Universidad de Chile (SSN: Servicio Sismológico Nacional), now the
104 National Seismological Center (CSN: Centro Sismológico Nacional, [Barrientos, 2018](#)). Using this network, the SSN
105 performed hypocentral location and magnitude estimation of the seismic swarm, including some earthquakes $M_l \sim 2$ -3
106 well recorded by near-field seismic stations (Fig. 2a and Fig. S2). The raw waveforms used for picking and locating
107 the earthquakes were archived by the SSN, including trimmed waveforms for 32 seismic stations and P-wave or S-wave
108 pick arrivals. In this study, we consider the CSN catalog due to the spatial station distribution and large gap window to
109 characterize the offshore swarm activity. This drawback does not allow us to improve the hypocentral locations using

110 algorithms such as the double-difference method. Unfortunately, there are no continuous records from these seismic
111 stations to search for microseismicity, except two broadband GSN (Global Seismological Network) stations: LCO (Las
112 Campanas) and LVC (Limón Verde), located 200 and 550 km-distance from the seismic swarm source, respectively
113 (see Fig. S2). Although both stations have good quality data, the long source-station distance and the significant data
114 gaps during the study period made it difficult to observe any small signal associated with the seismic swarm.

115 We aimed to assess for possible slip accelerations during the seismic swarm by analyzing the possible occurrence of
116 repetitive seismicity surrounding asperity areas. For this, we further attempted to study the presence of repeater and/or
117 near-repeating earthquakes in our catalog by performing cross-correlations between pairs of events. We considered
118 180 pairs of events recorded by the three components of the nearest stations CDCH, CRCH, and CPCH (Fig. 2a).
119 Afterward, we followed a standard pre-processing scheme involving detrending, tapering, bandpass filtering between
120 2 and 8 Hz, and resampling of the seismic signals. The chosen frequency band includes the corner frequency of
121 the entire seismicity of our dataset, which allowed us to characterize the repeater and/or near-repeating earthquakes
122 (Uchida, 2019; Uchida and Bürgmann, 2019) (see Fig. S4). We considered a time-window from 1 s before the P arrival
123 to 9 seconds after the S arrival of the normalized processed waveforms and correlate the pairs of events. Finally, we
124 took the maximum cross-correlation for the station and the arithmetic average among them.

125 **2.2. W-phase moment tensor inversion**

126 We computed the moment tensor and the centroid location of the two most significant earthquakes of the seismic
127 sequence, which occurred on April 30 at 19:17 and April 30 at 21:41 (hereafter first and second event). Thereby, we
128 performed a source inversion using the W-phase inversion algorithm (Duputel and Rivera, 2019). The algorithm fo-
129 cuses on finding the solution with the minimum root mean square (RMS) of the waveform misfits. We used teleseismic
130 waveforms from stations with an epicentral distance from 0° to 90° of the worldwide network Incorporated Research

131 Institutions for Seismology (IRIS, available at <http://ds.iris.edu/wilber3>, Fig. 2b). The time window used is
132 the standard for W-phase inversion, which begins with the P-wave arrival, and has a duration of $\delta t = 15 \times \Delta$, where
133 Δ corresponds to the epicentral distance. We filtered the data with a causal bandpass Butterworth filter of order 4.
134 The frequency band used corresponds to 100-250 sec and 100-200 sec for the first and second events, respectively.
135 We chose these frequency bands following the work of Duputel and Rivera (2019) and considering the signal-to-noise
136 ratio of each event.

137 To obtain the focal mechanism, we first performed an initial inversion using the solution given by the Global
138 Centroid Moment Tensor (GCMT, Ekström et al., 2012; Dziewonski et al., 1981) catalog as preliminary information.
139 We performed automatic and manual waveform selection to exclude noisy or incomplete data. After data screening,
140 solutions were obtained using 30 and 14 channels for the first and second event, respectively. We then performed
141 a second solution and iterated in space and time to determine the centroid position and W-phase moment magnitude
142 (M_{ww}). Once we have the best hypocentral location, we run the algorithm to compute the focal mechanism at different
143 depths to analyze the solutions.

144 2.3. GPS data

145 At the time of the 2006 seismic swarm, station COPO, located at a ~100 km distance eastward from the seismic
146 swarm source, was the only single available continuous GPS site operating in the Copiapó area (Fig. 2a). This site
147 was installed on 2002-07-01 and shut down on 2015-08-05 (Fig. S5). Although the COPO station has large gaps in its
148 records between 2007-10-01 and 2008-07-03, we detected a few days of data gaps during the 2006 seismic swarm: 2
149 days before and after the two largest earthquakes of the sequence.

150 We used the GPS time series from the database SOAM_GNSS_solENS (Klein et al., 2022b). This solution database
151 provides time series of precise daily station positions obtained from double-difference processing expressed with re-

152 spect to ITRF14. This dataset has been used recently to develop precise time-dependent afterslip evolution after large
153 earthquakes (Tissandier et al., 2023), as well as to identify transient signals along the northern Chile subduction zone
154 (Klein et al., 2022a). Here, we used a time-window from February to July 2006 for the horizontal components of the
155 COPO station; afterward, we detrended the COPO time series using the velocity estimated from 2 months before April
156 19, the date we identified as the beginning of the seismic swarm.

157 **2.4. InSAR data and modeling**

158 Synthetic Aperture Radar (SAR) data were acquired by the European Space Agency's ENVISAT satellite track 96.
159 Due to the sparse temporal coverage of the area, and the small magnitude of the deformation, a specific strategy has
160 to be used to separate tectonic signals from non-tectonic perturbations (tropospheric delays, ionospheric delays, and
161 orbital ramps). We computed interferograms with a small baseline strategy, requiring a closure of the interferometric
162 network while adapting the different steps to the irregular latitudinal coverage of the dataset (Fig. S6a). We first
163 coregistered all images with respect to a single primary image, using intermediate primary images to connect the
164 most distant acquisitions (in space and time, Fig. S6b). This constraint led us to include a total of 55 interferograms
165 with perpendicular baselines reaching up to 585 m and temporal baselines up to 5 years. To maintain an acceptable
166 level of coherence and facilitate phase unwrapping, we corrected the interferograms from DEM errors (Ducret et al.,
167 2013) and subtracted stratified atmospheric delays derived from ERA-Interim (Jolivet et al., 2011). After applying a
168 moving-average filter, we ran an iterative unwrapping procedure guided by coherence, as described in Grandin et al.
169 (2012).

170 Finally, after unwrapping, we estimated parameters of phase ramps in azimuth and in range, and inverted for
171 those parameters in a network fashion to ensure a consistent correction of all interferograms. Prior to parameter
172 estimation, interferograms were clipped to discard phase values evidently affected by a local atmospheric artifact, and

173 measurements in the area of the Copiapó swarm were masked to avoid contaminating the phase ramp estimation with
174 a potential tectonic signal. For the azimuth ramp, we used a cubic fit as a function of azimuth coordinate for “long”
175 interferograms (i.e. exceeding ~ 400 km along-track), whereas a quadratic fit was used for “short” interferograms.
176 Because the images are narrower in the range dimension, the orbital ramps in the range were modeled as linear.

177 After interferogram correction, the majority of atmospheric and orbital artifacts were expected to be mitigated.
178 However, the topography of the area is characterized by an east-west elevation gradient that translates, in the presence
179 of a strong stratified component of atmospheric delays, into a steep phase ramp in range. Hence, uncertainty on the
180 atmospheric corrections mapped into a bias in the empirical ramp corrections. In order to further improve the orbital
181 and atmospheric corrections, we performed a time-series inversion of the interferogram network, incorporating (1) a
182 smoothness constraint in time, (2) a linear phase-elevation term with a coefficient varying linearly with azimuth (to
183 account for the latitudinal change in atmospheric phase screen), and (3) a linear ramp in range with a coefficient varying
184 linearly with azimuth (which yields a skewed phase ramp).

185 **3. Results**

186 **3.1. Migration of seismicity**

187 The quality of the manual picks was good enough to identify the main characteristics of the seismic swarm. Using
188 the trimmed raw waveforms for 32 seismic stations (see Fig. S2), we were able to identify 2470 pick arrivals, either
189 P or S phases performed by the SSN, between February 28 and June 1 in the study area (Fig. 2), with a total of 312
190 events. We then used the hypocentral location of the seismicity, discriminating those earthquakes associated with the
191 seismic swarm both in space and time. Figure 3 shows the spatiotemporal evolution of the seismicity between April
192 and May 2006 associated with the Copiapó swarm; in this figure, the main reference is the event that occurred on
193 April 19, Ml 5.3, which we identified as the first event of the whole seismic swarm. After this event, all subsequent

194 seismicity during the next nine days occurred within a localized zone along latitude and longitude (Fig. 3b, and 3c,
195 respectively). The view of a clustered seismicity is also supported by the observed similarity in S-P time during the
196 same period at the coastal stations CDCH and CRCH; nonetheless, at inland station CPCH, these results are not clear
197 due to the long distance from the seismic swarm source (Fig. S3). Although the final catalog includes 235 events with
198 magnitudes between $M1.7-6.6$, the magnitude of completeness is about $M3.7$.

199 We calculated the radial distance from the epicentral position of the event that occurred on April 19 (Fig. 3d).
200 During this day, we observed a clustered seismicity propagated at fast velocities in both directions, eastward and
201 westward the first shock. However, following the next ten days after this cluster (Fig. 3d), we identified mainly two
202 patterns: (1) an eastward migration (greenish circles) at velocities between 2 to 10 km/day and (2) a westward migration
203 (pinkish circles) at velocities about 2 to 5 km/day. Interestingly, during the same period between April 19 to April 28,
204 we observed a slightly westward motion of about 2 mm in the time series of the GPS station COPO (Fig. 4). There
205 were no changes in the north-south component.

206 We further investigated possible additional signatures of slow deformation to support the slightly westward trend of
207 the COPO station. First, we studied the possible presence of repeating earthquakes, similar events, or doublets in our
208 database. We found doublet events in the frequency band between 2-8 Hz using the three closest stations to the seismic
209 swarm source. We obtained only four pairs of events with correlation coefficients greater than or equal to 0.85 (Fig. 5
210 and Fig. S7). The highly correlated doublet ($cc=0.97$) occurred on April 19, when we identified the beginning of the
211 seismic swarm, with two events magnitudes $M1.2.9$ and $M1.3.3$ (Fig. 5b). After considering all possible pairs of events
212 recorded by the three-component three stations CDCH, CPCH, and CRCH (in total, there are 180 earthquakes during
213 the period analyzed), we built a similarity matrix that contains the correlation coefficient for all the event numbers (Fig.
214 5a). Here, we noticed that during the first days of the seismic swarm, between April 19 and April 20, the correlation

215 coefficient was the highest of all the periods, including values larger than 0.5, suggesting highly clustered activity.
216 Overall, we retrieved doublets events and seismicity increase that could indicate the presence of slow slip in the area.
217 Although we expected the presence of repeater earthquakes through time, the high magnitude threshold and the lack
218 of continuous records reduce our detection capability of such signals.

219 On April 28 (day 9), a new series of earthquakes started, migrating southwest (pinkish circles on Fig. 3d) while
220 the clustered seismicity started spreading in latitude and longitude. Then, the spreading of the seismicity was mainly
221 affected by the two largest earthquakes of the whole sequence that occurred on April 30 at 19:17 UTC and 21:40
222 UTC. The earthquakes produce an offset of about 15 mm at the east-west component and 3 mm at the north-south
223 component of the COPO GPS station. We analyzed these earthquakes in section 3.2. On May 2 (day 13, Fig. 3d),
224 seismicity continues growing to the southwest, forming a secondary cluster near 71.6°W , 27.4°S (Fig. 3a). However,
225 during this period, we cannot observe any noteworthy trend in the COPO time series other than the postseismic afterslip
226 promoted by the two largest events mentioned above, mainly observed in the east-west component (Fig. 4).

227 **3.2. The two largest earthquakes within the swarm**

228 We studied the two largest events of the sequence. Both events magnitude $M_w \sim 6.5$ - 6.6 occurred on April 30, only
229 2.4 hours apart. Other seismological agencies, such as GCMT or NEIC, show substantial differences in the magnitude,
230 depth, and location of these earthquakes. The regional records at stations CDCH, CPCH, and CRCH (see Fig. S8)
231 show only minor amplitude, shape, and time signal differences. However, the regional data were insufficient to perform
232 this analysis; we employed a W-phase inversion using teleseismic records to characterize the seismic source of these
233 events.

234 The inversion solution localizes the centroid of the first event at 27.17°S , 71.3°W and the second event at 27.08°S ,
235 71.33°W (Fig. S9a, c). The iteration in time shows that the time shift corresponds to 6.0s and 7.0s for the first and

236 second events, respectively (Fig. S9b, d). The waveform fit of each solution is shown in the supplementary material
237 in Fig. S10 (for the first event) and Fig. S11 (for the second event). Furthermore, Fig. 6 summarizes the W-phase
238 inversion of the first and second events. The figure shows the focal mechanism of the earthquakes at different depths as
239 a function of the normalized root mean square misfit $\left(\frac{rms}{min(rms)} \times 100\right)$ and the best solution in each case. Around the
240 best-fit solutions, the obtained moment tensor is similar. Moreover, the first event depth between 11-17 km presents
241 the lowest misfit values (Fig. 6a), while for the second event, the lower misfit appears in the range between 23-35 km
242 depth (Fig. 6b). The differences in the depth range might be due to the low signal-to-noise ratio, in addition to the
243 poor quality seismograms recorded for the second event, which are mixed with the surface waves of the first event.
244 Fig. 6c, d also shows that the rupture mechanism of both events corresponds to a reverse fault with a magnitude M_{ww}
245 6.56 and M_{ww} 6.5, respectively.

246 3.3. Coseismic and Postseismic deformation from InSAR and GNSS data

247 The result of the time-series inversion, after removing the atmospheric and orbital components, is displayed in Fig.
248 S12, plotted using reference images before (Fig. S12a) and after (Fig. S12b) the 2006 Copiapó swarm. The difference
249 in deformation that occurred between the two consecutive acquisitions, bracketing the time of the Copiapó swarm, is
250 evident (2005-09-26 and 2006-07-03). However, the long temporal window between these images hinders a detailed
251 quantification of this deformation event.

252 We also observed that deformation continued during the two time periods that followed the main time-step of it
253 (between 2006-07-03 and 2006-08-07, and between 2006-08-07 and 2007-03-05). This observation is consistent with
254 the abnormal motion detected at GPS station COPO in the ~6 months following the swarm (Fig. 2 and 4). In order
255 to further separate this instantaneous deformation from an additional transient signal, we applied a parametric pixel-
256 wise inversion of the cumulative deformation time series (after discarding non-tectonic signals). We assumed that the

257 time-series consists in the superposition of (1) a Heaviside function at the time of the earthquake (the “coseismic” com-
258 ponent), (2) a linear transient taking place in a time-interval of finite duration after the earthquake (the “postseismic”
259 component) and (3) a constant (the “reference image” phase screen). We did not incorporate an interseismic trend in
260 the inversion to avoid a trade-off with the postseismic component, whereas accounting for a more realistic temporal
261 evolution of the postseismic transient (logarithmic, exponential) leads to similar results for the total displacement of
262 the transient.

263 The result of this signal separation procedure is shown in Fig. S13. The coseismic component is characterized by
264 increasing displacement (away from the satellite) towards the area affected by the Copiapó swarm, reaching a maximum
265 of approximately 5 cm in the LOS at the coast. The postseismic component has a similar spatial distribution, albeit
266 peaking inland, with a smaller displacement (maximum 3 cm). This result is consistent with the analysis of [Holtkamp
267 et al. \(2011\)](#), although our exhaustive exploitation of the whole ENVISAT dataset allows for a better separation of
268 signals. Based on their spatial pattern, both the co- and postseismic patterns are consistent with slip on the subduction
269 interface taking place offshore or under the coast at the latitude of the Copiapó swarm.

270 In order to quantify the spatial distribution of slip associated with the co- and post-seismic components, we invert
271 for slip on the subduction interface, incorporating both the InSAR-derived displacements and the displacement esti-
272 mated from GPS station COPO. For the latter estimation, we extract the horizontal vectors in the two time intervals
273 defined from the InSAR temporal coverage by fitting the same temporal functions (interseismic trend, coseismic step,
274 postseismic transient) on the COPO time series. We obtain a “coseismic” displacement of -1.6 cm EW and 0.4 cm NS,
275 and a “postseismic” displacement of -0.7 cm EW and -0.2 cm NS (with 1-sigma uncertainties of 0.2 cm). The inversion
276 uses the equations of [Okada \(1985\)](#), following the same approach presented by [Ruiz et al. \(2013\)](#). However, the small
277 signal-to-noise ratio of the InSAR and GNSS datasets requires to incorporate constraints in the inversion to mitigate

278 instabilities. We choose to apply a total seismic moment constraint, whereby the integrated slip on the interface has to
279 match a prescribed geodetic moment (which can be converted to a seismic moment by multiplying by an appropriate
280 value of the shear modulus). For the “coseismic” inversion, we force the slip distribution to match a seismic moment
281 of $2.3 \cdot 10^{19}$ Nm (assuming a shear modulus of 30 GPa), which corresponds to the cumulative seismic moment released
282 during the “coseismic” phase (representing an equivalent magnitude Mw 6.8). For the “postseismic” inversion (after
283 2006-07-03), the cumulative seismic moment released by local earthquakes (equivalent to Mw 5.4) is insufficient to
284 match the quantity of deformation measured at the surface, unless slip is occurring at a depth substantially shallower
285 than the plate interface. As a consequence, to comply with the assumption that slip is taking place on the interface, we
286 enhance the seismic moment constraint so as to match an equivalent magnitude Mw 6.5.

287 The resulting slip distributions, as well as synthetic displacement maps, are shown in Fig. 7. Slip during the
288 “coseismic” phase reaches 40 cm and is constrained between the coast and halfway to the trench. On the other hand,
289 “postseismic” slip occurs on a narrow band aligned along the coast. However, the precise slip distribution remains
290 poorly resolved, especially in its up-dip segment of the subduction interface.

291 4. Discussion

292 4.1. Seismic swarm migration and the two largest earthquakes

293 We analyzed the spatial and temporal evolution of the Copiapó swarm from the day of the first earthquake, the Ml
294 5.3 occurred on April 19, until April 30. In the early stage, the sequence exhibits localized and persistent seismicity
295 in the central area of the whole seismic swarm (Fig. 3a). The epicentral location of these earthquakes is well resolved
296 due to the small latitude and longitude errors (see Fig. S14). The intense clustered seismicity can be interpreted as a
297 burst of seismicity during the first day with a fast migration, likely following an earthquake cascade interaction among
298 small events. After that phase, during the next ten days, the seismicity follows mainly two trends; one toward the

299 east of the location of the first event (greenish circles on Fig. 3d), characterized by high seismicity that migrates at
300 velocities between 2–10 km/day; a second trend toward the trench (pinkish circles on Fig. 3d) that seems to migrate
301 at lower velocities around 2–5 km/day. On the other hand, we further studied the possibility of seismicity migration
302 rates induced by a fluid diffusion migration [Shapiro et al. \(1997\)](#). Fig. 3d shows the fluid diffusion curves considering
303 hydraulic diffusivity of 100, 200, and 300 m²/s to explain the data. Similar curves have been obtained by [Shapiro](#)
304 [et al. \(2003\)](#), who proposed these values as an upper limit for the diffusivity coefficient. In addition, the fluid diffusion
305 processes are expected to be slower than 0.5 km/day, while slow slip fronts show velocities of about a few 3–10 km/day
306 ([Hoskins et al., 2021](#)). Thus, these migration velocities are compatible with a slow slip event propagation in subduction
307 zones (e.g., [Shelly et al., 2007](#); [Kato et al., 2016](#)).

308 The migration pattern described above continued until April 30 (day 11), when the two largest earthquakes of the
309 sequence ruptured to the west of the April 19 event. First, at 19:17 (UTC), the earthquake magnitude Mw 6.6 ruptured
310 at shallow depths of around 15 km with an epicentral location at mid-distance between the trench and the coastline.
311 According to the slab 2.0 model, the earthquake occurred at the plate interface. Seismicity followed this earthquake
312 until 144 min after when the second event of magnitude Mw 6.5 ruptured only ~10 km to the northwest from the
313 first event. Due to the closeness of these largest earthquakes, and also considering their rupture size, they could have
314 interacted between them by a triggering process led by the redistribution of stress. After these events (exceeding the
315 magnitude of the whole swarm), the seismicity exhibits a more organized pattern with an acceleration in the cumulative
316 number of events. Moreover, the persistent and localized seismicity that occurred during the initial period vanished.
317 We instead observe that the seismicity spreads along an apparent north-east to south-west alignment (Fig. 3), which
318 may be connected to the track of the subducted Copiapó ridge and its deformation fingerprint along the plate interface
319 and the overriding plate ([Álvarez et al., 2015](#)). Finally, during the last period until mid-May, the seismicity is likely

320 driven by the afterslip triggered by the two April 30 Mw~6.5-6.6 earthquakes.

321 One question that needs to be addressed is whether the 2006 Copiapó crisis follows the characteristics of a seismic
322 swarm or rather shows a pattern of mainshock–aftershock. Despite our previous observations on the spatiotemporal
323 seismicity evolution, we agree with [Holtkamp et al. \(2011\)](#) that the 2006 Copiapó crisis as a whole could be described
324 as a seismic swarm; firstly, the largest earthquakes in the sequence occurred in the middle of the sequence; secondly,
325 the total area of the seismic swarm, about 100 km-long and 70 km-wide, is much larger than one would expect given
326 the size of the earthquakes involved in the sequence; and finally, the migration described above suggests that additional
327 aseismic processes drove seismicity to spread over a wider area during over three weeks.

328 A key question remains on the depth of the seismicity, and the main earthquakes analyzed here. The regional
329 network was limited in 2006; therefore, the depth accuracy is poorly constrained in the studied seismic catalog. The
330 first events of the seismic swarm have low-depth uncertainties; however, we acknowledge that our scarce database did
331 not allow us to obtain a high-resolution picture offshore, only using the information from a few inland stations. Based
332 on the analysis of the two largest earthquakes of the sequence using teleseismic information, we can constrain the depth
333 location of the two largest earthquakes of the sequence. For the first event, the solution converges to ~15 km depth,
334 while the second event shows similar Normalized RMS misfits for a wider depth range, a problem likely induced by
335 seismic ambient noise ([Morales-Yáñez et al., 2020](#)) due to the first event. Nonetheless, a shallower solution may be
336 reliable considering also the uncertainties in the centroid depth (Fig. 6). Additionally, for all the possible estimations
337 in-depth, both reverse focal mechanisms indicate a low-angle rupture likely associated with the fault plane. Based on
338 our results, we suggest that the 2006 seismic swarm aforementioned occurred at the megathrust interface. However,
339 we cannot discard the possibility of shallow seismicity occurring in the overriding plate.

340 4.2. Slow & fast slip during the Copiapó swarm

341 Earthquake swarms along the Chilean subduction zone have occurred in a diversity of modes through seismic
342 sequences. These seismic swarms have been part of slow and fast behaviors at the plate interface, such as during the
343 Mw 8.1 2014 Iquique and the Mw 6.9 2017 Valparaíso (e.g., [Kato et al., 2016](#); [Ruiz et al., 2014, 2017](#); [Caballero](#)
344 [et al., 2021](#)). Conversely, other seismic swarms have been identified without a subsequent major event, such as the
345 recurrent Navidad swarm in Central-South Chile ([Valenzuela-Malebrán et al., 2021](#)) or some persistent seismic swarms
346 occurring in the Coquimbo region, North-Central Chile ([Poli et al., 2017](#); [Vigny et al., 2009](#)) that exhibit moderate-to-
347 low magnitude earthquakes.

348 The single GPS station COPO was analyzed to address if any transient signal took place during the period of the
349 2006 Copiapó swarm (Fig. 4). We identified a slightly westward/trenchward transient from April 19 to April 28.
350 Precisely, this small trend change started the same day we identified the beginning of the seismic swarm while we
351 observed a burst of seismicity occurring on April 19. Moreover, during this period, we observe higher waveform
352 similarities between pairs of earthquakes, including doublets with a high correlation coefficient as a potential repeater
353 event (Fig. 5 and Fig. S7). We consider that this intensive doublet activity and the seismic swarm evolution in this
354 first stage took place while an SSE had driven slip on the plate interface. The relative depth of the seismicity, which
355 according to the epicentral location, could reach 15–20 km depth, suggests that this potential SSE took place at a
356 shallow segment of the megathrust. The possible short-term SSE is not comparable to the Mexican (e.g. [Radiguet](#)
357 [et al., 2012](#)), Cascadia (e.g. [Bletery and Nocquet, 2020](#)), or New Zealand (e.g. [Wallace et al., 2012](#)) transient signals
358 that could reach a few centimeters of displacement due to the scarce GPS instrumentation at this time. Based on our
359 findings, we propose that a $M\sim 6$ SSE is feasible offshore along the shallowest segment of the plate interface. Around
360 La Plata Island, Ecuador, [Vallée et al. \(2013\)](#) documented shallow SSE together with seismic swarms likely driven by

361 stress fluctuations related to aseismic slip and supported by consistent families of repetitive earthquakes. Observations
362 such as in Ecuador may indicate that seismic swarm activity and slow processes have a key role in stress release along
363 subduction zones, and possibly these processes occur synchronously.

364 To further analyze the influence of the proposed SSE, we perform the inversion of the coseismic deformation of
365 the 2006 seismic swarm from both GPS and InSAR observations (Fig. 7). We assume that the slip takes place on the
366 subduction interface, and we carried out an exploration of parameters on the area of the dislocation. Our results are
367 shown in Fig. 7a and Fig. S15. The parameters that best fit the data are a slip distribution of dimensions of about
368 $26 \times 35 \text{ km}$ and a maximum slip of 40 cm, located in an area that agrees with our focal mechanism solutions. This
369 coseismic slip distribution considers a whole period that we so-called “coseismic”, but includes mainly the seismic
370 swarm and the two largest earthquakes magnitude $M_w \sim 6.5-6.6$. We also estimated the geodetic moment from our
371 inversion, equivalent to an $M_w 6.85$, compared to the cumulative seismic moment released in the same period, equal
372 to an $M_w 6.77$. Following these results, during the coseismic period, we observed both seismic and aseismic slips
373 but no strong differences between them in terms of total moment released. Previously, [Holtkamp et al. \(2011\)](#) also
374 performed the inversion of the coseismic deformation with only three interferograms and indicated that the model that
375 best explains their data does not require a significant aseismic motion. However, their results show a strong residual
376 inland around the Copiapó city that could be controlled for an important postseismic component included as a dataset
377 of their inversion. This example motivates us to separate the postseismic contribution from the coseismic component
378 by carefully studying the temporal inversion from a set of 55 interferograms. Our results are shown in Fig. 7b and Fig.
379 S16. Our best solution shows a dislocation taking place deeper and slightly further south than the coseismic rupture,
380 with an average slip of about 26.5 cm. The estimated geodetic moment is equivalent to an $M_w 6.6$, a value several
381 times greater than the cumulative seismic moment from this period equivalent to an $M_w 5.4$. These results lead us to

382 interpret the postseismic slip occurring along the plate interface with a significant aseismic component of about 98%,
383 which had not been highlighted before.

384 An interesting interplay between seismic and aseismic deformation during swarm episodes has been proposed for
385 some segments of the South America subduction. For instance, in North-Central Chile, [Klein et al. \(2021\)](#) analyzed the
386 estimated moment released by the 2020 Atacama seismic sequence, which was 60% due to earthquakes and 40% due to
387 aseismic slip in an area of about $100 \times 100 \text{ km}^2$. Also, in Chile, during the nucleation phase of the Mw 6.9 Valparaíso
388 earthquake sequence, [Ruiz et al. \(2017\)](#) proposed about 80% of aseismic slip released; conversely, [Caballero et al.](#)
389 [\(2021\)](#) estimated about $51\% \pm 11\%$ of aseismic slip on the megathrust. Moreover, in northern Peru, a shallow seismic
390 sequence that occurred in 2009 was accompanied by an SSE that lasted seven months ([Villegas-Lanza et al., 2016](#)).
391 Given the moment released, the authors suggested that a 70%–85% aseismic process occurred in an area of about 80
392 $\times 80 \text{ km}^2$. In northern Ecuador, the 2013–2014 seismic swarm was jointly detected by an SSE, with the evolution of
393 aseismic slip representing 99% of the total moment released ([Vaca et al., 2018](#)). Finally, [Segovia et al. \(2018\)](#) also
394 found on La Plata Island, Ecuador, that the 2013 seismic swarm was synchronous with an SSE that released about
395 80% of the total moment estimated from geodetic motion. For the 2006 Copiapó swarm, we roughly estimate a ratio
396 of the overall seismic and aseismic moment released of about 43% and 57%, respectively, which occurred in a large
397 area of $100 \times 70 \text{ km}^2$. These relatively moderate **M**6–7 magnitude sequences occurred in large areas considering
398 the maximum magnitude earthquake of their whole sequences. In summary, although the seismic and aseismic ratio
399 differences for these seismic swarm episodes in the South America subduction zone, similar mechanisms, such as slow
400 slip deformation, seem to appear in most of them, suggesting a common driver of microseismicity in large extensions
401 in which seismic swarms occur.

402 We synthesized our insights in Fig. 8, which include the seismic swarm, the two largest earthquakes, and the

403 seismicity after these two major events; we also include the coseismic and postseismic deformation associated with
404 the 2006 Copiapó swarm, as well as other aseismic signatures discovered in the area such as non-volcanic tremors
405 (NVT) and the possible 2005 deep SSE (Pastén-Araya et al., 2022; Klein et al., 2018a). Considering the Lay et al.
406 (2012) subduction earthquake classification, here we followed the most specific along-dip segmentation for this region
407 proposed by Pastén-Araya et al. (2022). We observed that the recurrent deep SSE in 2005, 2009, and 2014 took place in
408 a deeper segment of the megathrust in zone C, and the NVT activity seems to occur in zone B referred as a transitional
409 segment that may impede the propagation of major ruptures; whereas the synchronous seismic swarm and slow slip
410 event, including doublets events, and the spreading of the seismicity, occurred at shallow depths in zone A, the same
411 area where similar events and potential repeater earthquakes were previously identified (Pastén-Araya et al., 2022).
412 These aseismic signatures proposed in our work add another intriguing component to the diversity of slip behaviors
413 previously reported in the Atacama region.

414 **4.3. The influence of the Copiapó Ridge**

415 The presence of remarkable high-bathymetric features in the oceanic lithosphere as the Copiapó Ridge and its
416 seamounts subducting may play a role in the subduction processes inducing frictional segmentation along the plate
417 interface and their surroundings (Wang and Bilek, 2011, 2014). The effects include coupling coefficient differences,
418 a wide diversity of slip behaviors, and seismic/aseismic signatures along the plate interface, resulting in a decrease of
419 normal stress potentially driven by fluid pressure (Poli et al., 2017). Therefore, the complexities and heterogeneities at
420 these depths favor aseismic creep, seismic swarm, and repeater activity (Wang and Bilek, 2011; Valenzuela-Malebrán
421 et al., 2021; Singh et al., 2011). In Copiapó, Chile, Pastén-Araya et al. (2022) inferred an along-dip heterogeneous plate
422 interface, identifying clusters of similar events at shallow depths in the interface (between 18 to 29 km depth) occurring
423 in a zone with a high V_p/V_s ratio and moderate V_s and V_p values, and with a low coupling value (Klein et al., 2018b;

424 [Metois et al., 2016](#)), separating two areas of high coupling northern and southern the path of the seamounts tracking.
425 Moreover, the 2006 Copiapó swarm occurred at the edge of a low coupling zone, which favors our hypothesis of an
426 SSE occurring just below this shallowest segment of the plate interface where also NVT activity has been identified.
427 These physical conditions suggest fluid content in the system that may drive or promote transient aseismic slip at that
428 portion of the megathrust.

429 More recently, in Central Chile, the 2017 Valparaíso Mw 6.9 earthquake nucleated in the vicinity of a subducted
430 seamount of the Juan Fernández Ridge ([Ruiz et al., 2018](#)). In this case, the clustered seismicity presented a migra-
431 tion pattern from the north to the south-east, potentially associated with an aseismic slip transient ([Ruiz et al., 2017](#);
432 [Caballero et al., 2021](#)). The similar nature and migration history between the Copiapó Ridge and the Juan Fernández
433 Ridge ([Bello-González et al., 2018](#)), suggest a similar influence on the slip behaviors due to the seamounts subducted
434 for each Ridge. In both cases, the high topographic complexities, seismicity migration, and potential aseismic pro-
435 cess reflect an asperity-like behavior that may promote clustered low-to-moderate seismicity but also changes in the
436 deformation process along the plate interface.

437 Subducted oceanic features such as oceanic ridges also indicate potential fractures of the upper plate around the
438 subducting seamounts within the forearc regions ([Wang and Bilek, 2011](#); [Morell, 2016](#)). For instance, in the Ecuadorian
439 subduction zone, [Collot et al. \(2017\)](#) studied how the oceanic relief subducting is deforming seismic and aseismically
440 the forearc in an area of recurrent SSE located in a partly locked region. They described that seismicity could rupture at
441 the plate interface, and other events could reactivate near faults, while an SSE induces a stress increment and promotes
442 complex and multiple ruptures in the seamount's surroundings. If that is the case of the 2006 Copiapó swarm, we
443 think that the persistent and localized seismic swarm during the first period may occur at shallow depths, possibly
444 influenced by a seamount undergoing subduction as suggested by ([Comte et al., 2002](#)). The spatial location of this

445 seamount along the interface could explain the seafloor morphology observed in the bathymetry as a response to the
446 seamount subducting in the area (Métois et al., 2014; Comte et al., 2006). Therefore, following other authors, we
447 consider that the tracking of the Copiapó Ridge and the spatial distribution of their seamounts may influence and
448 trigger the diversity of seismic and aseismic signatures observed, including the 2006 seismic swarm.

449 5. Conclusion

450 We have studied the fast and slow processes related to the 2006 Copiapó swarm performing seismological and
451 geodetic constraints. The seismic swarm occurred at a shallow area of the plate interface that spatially correlates with
452 an inferred subducted seamount of the Copiapó Ridge at this latitude. We show a spatiotemporal evolution of the
453 seismicity, starting with clustered earthquakes on April 19 that migrate at velocities around 2 to 10 km/day until April
454 28, the same period when we find high cross-correlation coefficients among pairs of events, doublets earthquakes,
455 and a slight westward transient in the GPS station COPO. We further study the two largest earthquakes $M_w \sim 6.5$ – 6.6
456 that occur only 2.4 h apart from each other. The focal mechanism, centroid depth, and time shift solutions allow
457 us to propose similarities between them, confirming a low-angle mechanism, shallow depths constrained to the plate
458 interface, and similar rupture patterns. We characterized the coseismic and postseismic deformation related to the
459 seismic swarm by using InSAR images, from which we conclude a significant contribution of aseismic slip during the
460 postseismic period, while during the coseismic period, we identify a more negligible contribution. We proposed that
461 the 2006 Copiapó swarm and their migration patterns observed during the initial period were driven by a potential slow
462 slip event likely influenced by the presence of the Copiapó Ridge, which decoupled the plate interface and promoted
463 aseismic signatures such as NVT, repetitive earthquakes, and shallow and deep SSE, previously studied. Finally,
464 despite the data limitations during this period, we further attempt to study the large seismic swarm hosted in an area
465 where large earthquakes such as the 1922 Atacama event have occurred and where it has been a challenge to assess for

466 seismic hazard evaluation, including the potential influence of the slip behavior diversity.

467 **CRedit authorship contribution statement**

468 **Javier Ojeda:** Conceptualization of this study, Formal analysis, Investigation, Methodology, Software, Visual-
469 ization, Writing - original draft. **Catalina Morales-Yáñez:** Data curation, Formal analysis, Methodology, Software,
470 Writing - Original draft preparation. **Gabriel Ducret:** Data curation, Methodology, Writing - review & editing. **Sergio**
471 **Ruiz:** Conceptualization, Formal analysis, Investigation, Supervision, Writing - Original draft preparation. **Raphael**
472 **Grandin:** Data curation, Formal analysis, Methodology, Writing - Original draft preparation. **Marie-Pierre Doin:**
473 Methodology, Writing - review & editing. **Christophe Vigny:** Writing - review & editing. **Jean-Mathieu Nocquet:**
474 Formal analysis, Investigation, Writing - review & editing.

475 **Declaration of competing interest**

476 The authors declare that they have no known competing financial interests or personal relationships that could have
477 appeared to influence the work reported in this paper.

478 **Acknowledgments**

479 We wish to thank the network and station operators for their commitment to collect high-quality seismic data. The
480 seismic catalog was provided by the Centro Sismológico Nacional (CSN, Chile; <http://www.sismologia.cl/>, last
481 accessed 2022 May 31). Seismological data and metadata were accessed through the IRIS web service; we used
482 a combination of channels from GEOFON (GE), GEOSCOPE (G), ASL/USGS (IU,GT), IRIS/IDA (II), Pacific21
483 (PS) and BDSN (BK). The processing, mapping, and visualization of this article were benefited from various python
484 packages, including matplotlib (Hunter, 2007), obspy (Krischer et al., 2015), and pygmt (Uieda et al., 2021, using
485 3 arc second global relief from SRTM3S). JO acknowledges support from the Agencia Nacional de Investigación
486 y Desarrollo scholarship ANID-PFCHA/Doctorado Nacional/2020-21200903. CMY acknowledges funding from
487 ANID/FONDECYT 3220307 and thanks the support of the Anillo precursor project ANID PIA Anillo ACT192169.
488 SR thanks ANID/FONDECYT project no. 1200779. We thank the Agence Nationale de la Recherche (ANR), S5
489 project: “Synchronous Slow Slip & Seismic Swarm,” grant ANR-19-CE31-0003-01. Finally, the authors thank two
490 anonymous reviewers and the Editor, E. Contreras-Reyes, for their constructive comments and suggestions that helped
491 us to improve the original manuscript.

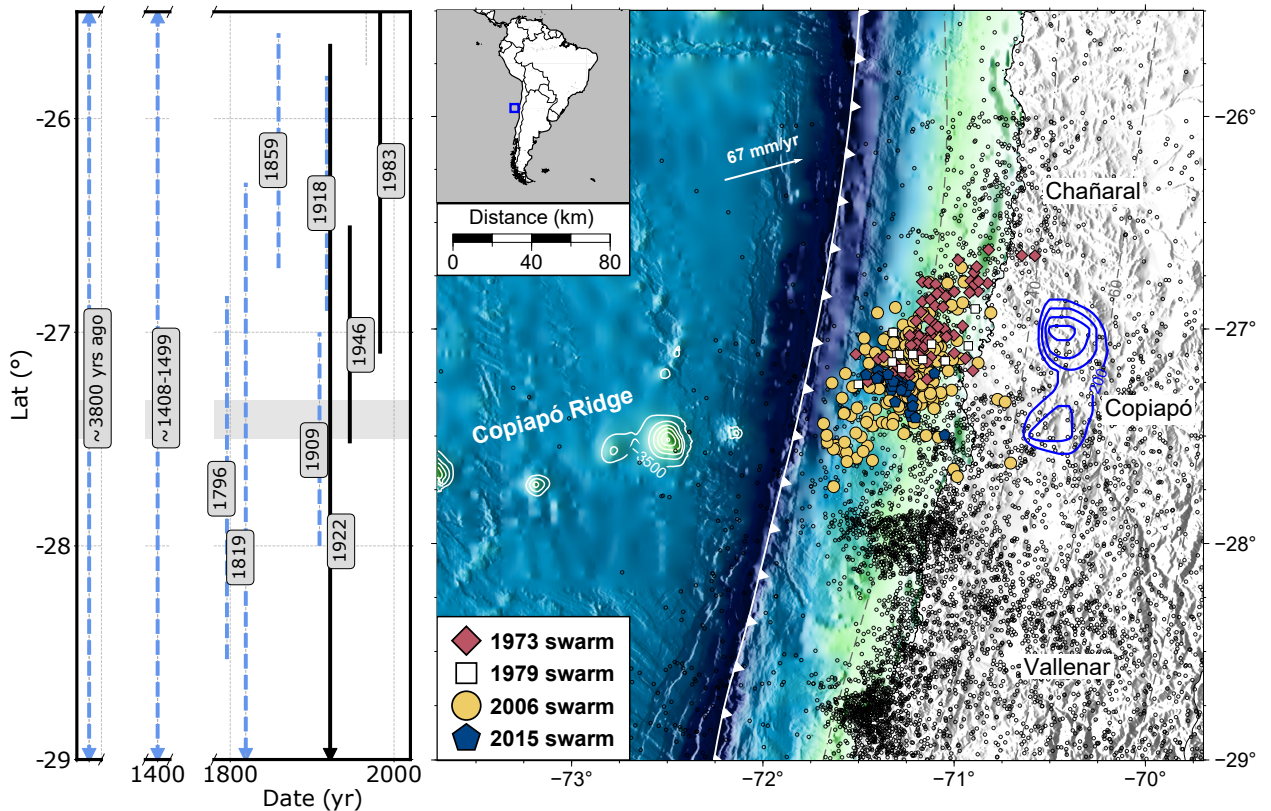


Figure 1: Overview of the study area; see the inset map showing the location with reference to South America. The segmented blue lines in the left panel indicate the rupture length of pre-historic, historical, and recent earthquakes (Comte et al., 2002; Ruiz and Madariaga, 2018; Abad et al., 2020; Salazar et al., 2022). The right panel indicates the seismotectonic context in the Copiapó region. The red, white, yellow, and blue circles indicate the seismicity location of the 1973, 1979, 2006, and 2015 seismic swarms, respectively. The gray dots indicate the seismicity that occurred between 1900 and 2022, database compiled by USGS and CSN. The blue lines are the 50 mm iso-contour slip of the 2014 deep SSE (Klein et al., 2018a). The white lines on the bathymetry indicate the 500 m iso-contours depth of the heterogeneous seamounts associated with the Copiapó Ridge. The white triangles indicate the trench, and the segmented black lines represent the Slab2 model of the South America subduction zone (Hayes et al., 2018).

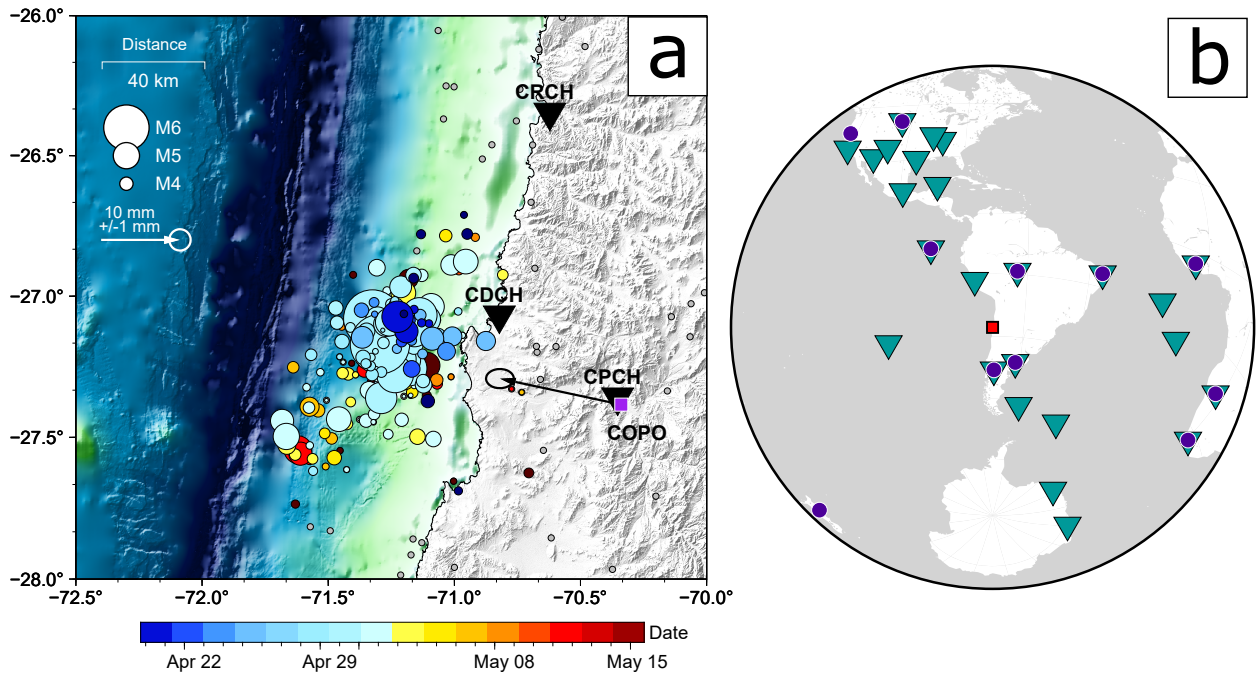


Figure 2: Available datasets during the 2006 Copiapó swarm. (a) The black inverse triangles are the regional short-period, three-component seismic stations; the purple square is the GPS station installed in Copiapó. The arrow and ellipse indicate the horizontal displacement due to the $M \sim 6.5$ earthquakes on April 30 and the respective horizontal error (Klein et al., 2022b). The circles represent the seismicity between 2006-04-19 and 2006-05-15, colored by the date of occurrence during the seismic swarm and sized by the magnitude of each event; gray dots are seismicity not related to the swarm. (b) Distribution of teleseismic stations used in the W-phase inversion for the two largest events of the seismic swarm: bright cyan inverted triangles for the 2006-04-30 19:17 event and purple circle for the 2006-04-30 21:40 event.

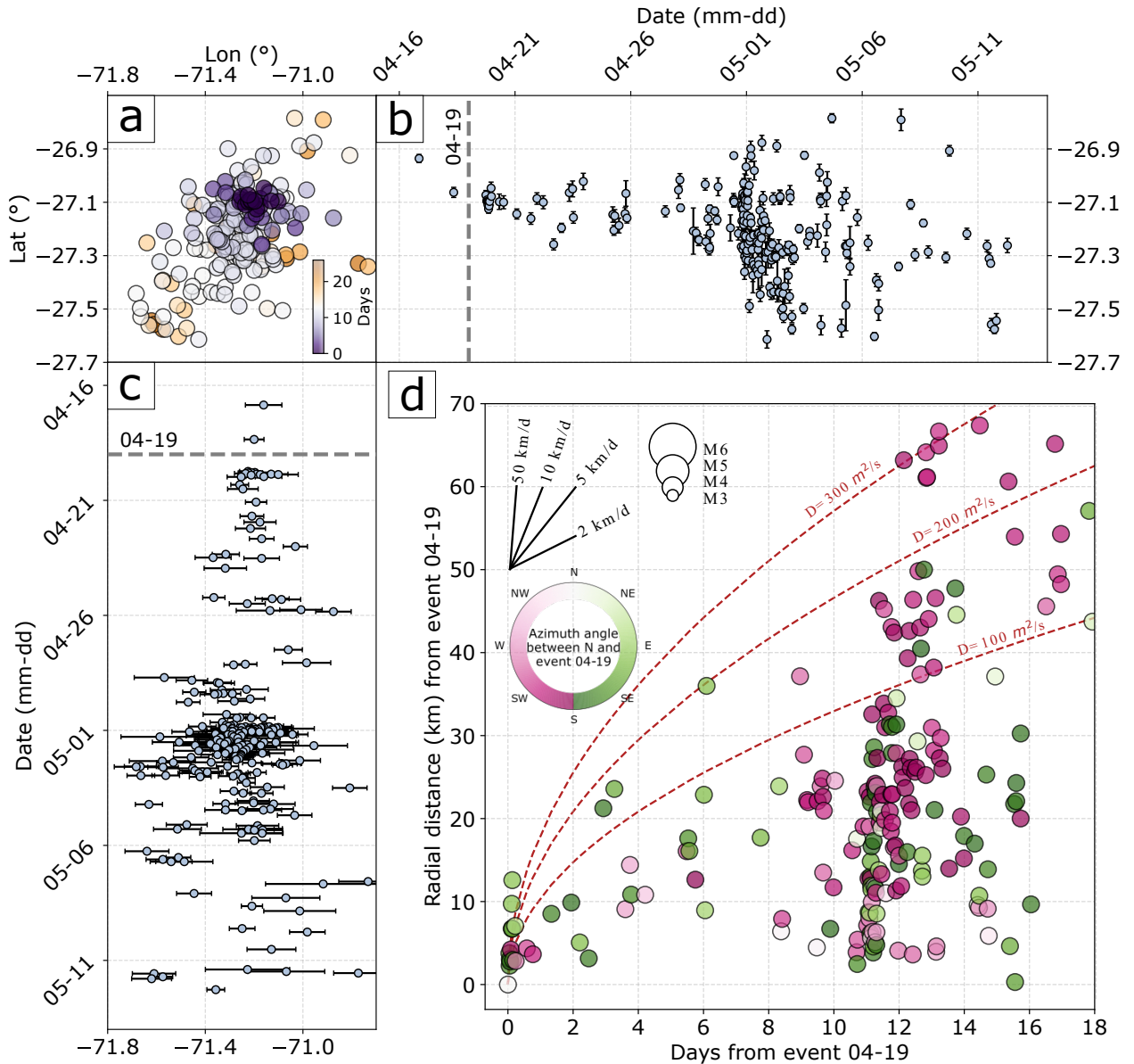


Figure 3: Spatiotemporal analysis of the 2006 Copiapó swarm. (a) Aerial view of the seismicity colored by date and sized by magnitude. The seismicity evolution from mid-April to June is indicated by (b) latitude in blue circles and (c) longitude in red circles; error bars are indicated for each event. (d) Radial spatial migration (measured from the event 2006-04-19) as a function of days. The black lines indicate migration velocities of 2, 5, 10, and 50 km/day. Red dashed lines are the fluid diffusion curves from Shapiro et al. (1997) using a hydraulic diffusivity (D) of 100, 200, and 300 m^2/s , representing the 98-, 95-, and 82-percentile of the seismicity, respectively. The white circle indicates the magnitude of the earthquakes from MI 3 to MI 6. The color of each circle is related to the azimuth angle between the N and the position of the 2006-04-19 event, as shown in the polar colorbar.

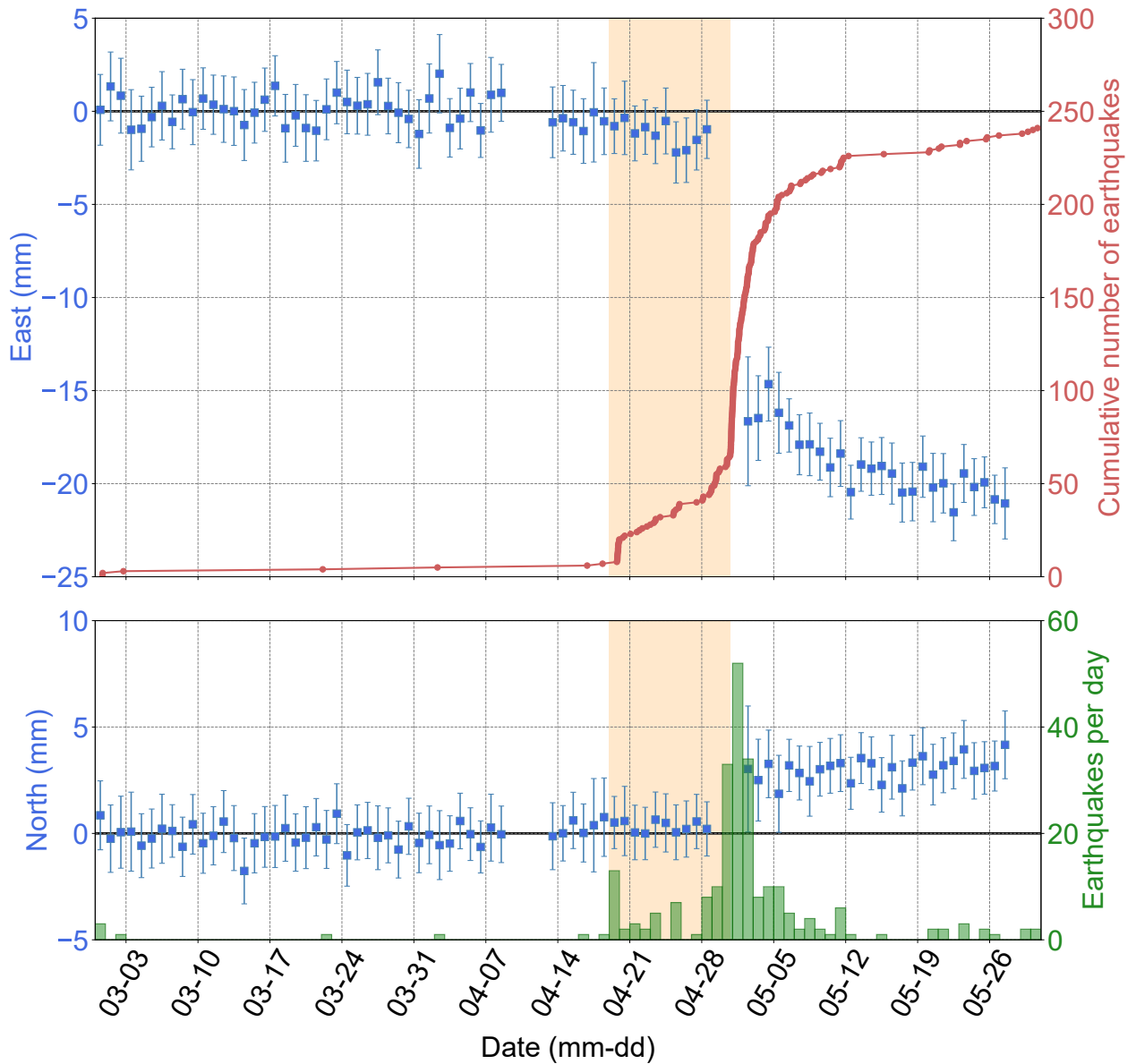


Figure 4: GPS displacement at station COPO for the east-west and north-south components (blue squares of top and bottom panels, respectively), error bars are indicated for each daily solution. The red curve (top panel) and green curve (bottom panel) correspond to the cumulative number of earthquakes and earthquakes per day, respectively. The orange area shows the period 2006-04-19 and 2006-04-30, before the largest earthquakes of the seismic sequence.

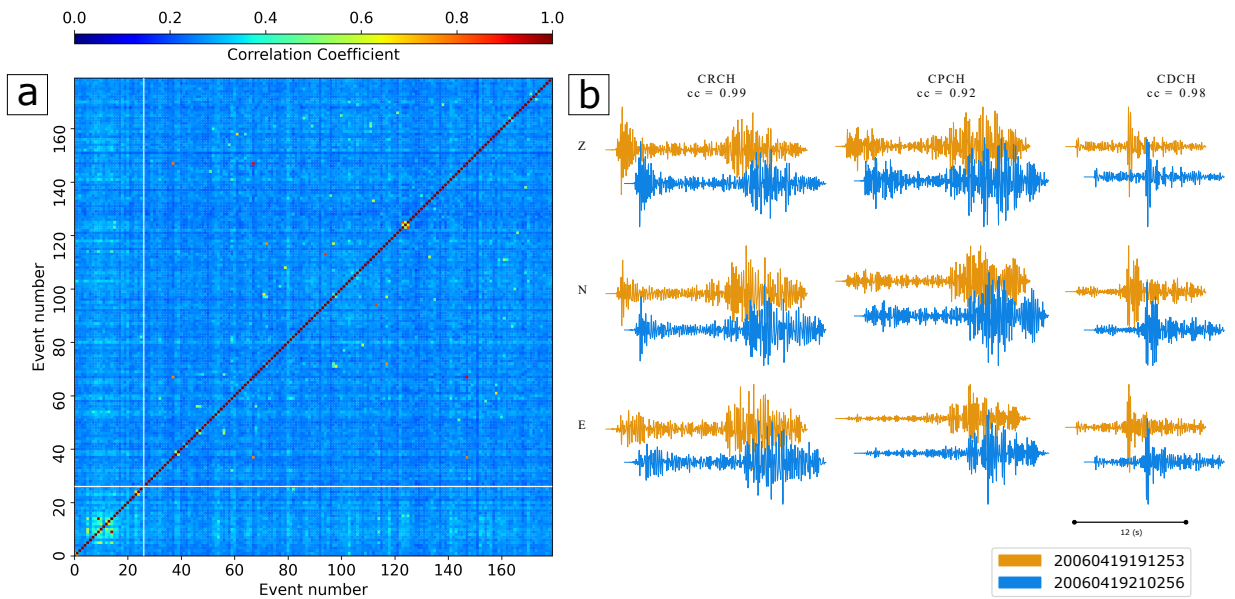


Figure 5: Analysis of doublets within the seismic swarm. (a) Similarity matrix for 180 pairs of events recorded by the three closest stations CDCH, CPCH, and CRCH. The Event number is sorted by the origin time of events. Event 0 and Event 180 correspond to the 2006-02-28 and 2006-06-01 events, respectively. The vertical and horizontal white lines indicate the event 2006-04-22 16:03:29. (b) Example of doublet for the Copiapó swarm, with a correlation coefficient larger than 0.97 considering three-components waveform cross-correlation. Pair (2006-04-19 19:12:53, 2006-04-19 21:02:56).

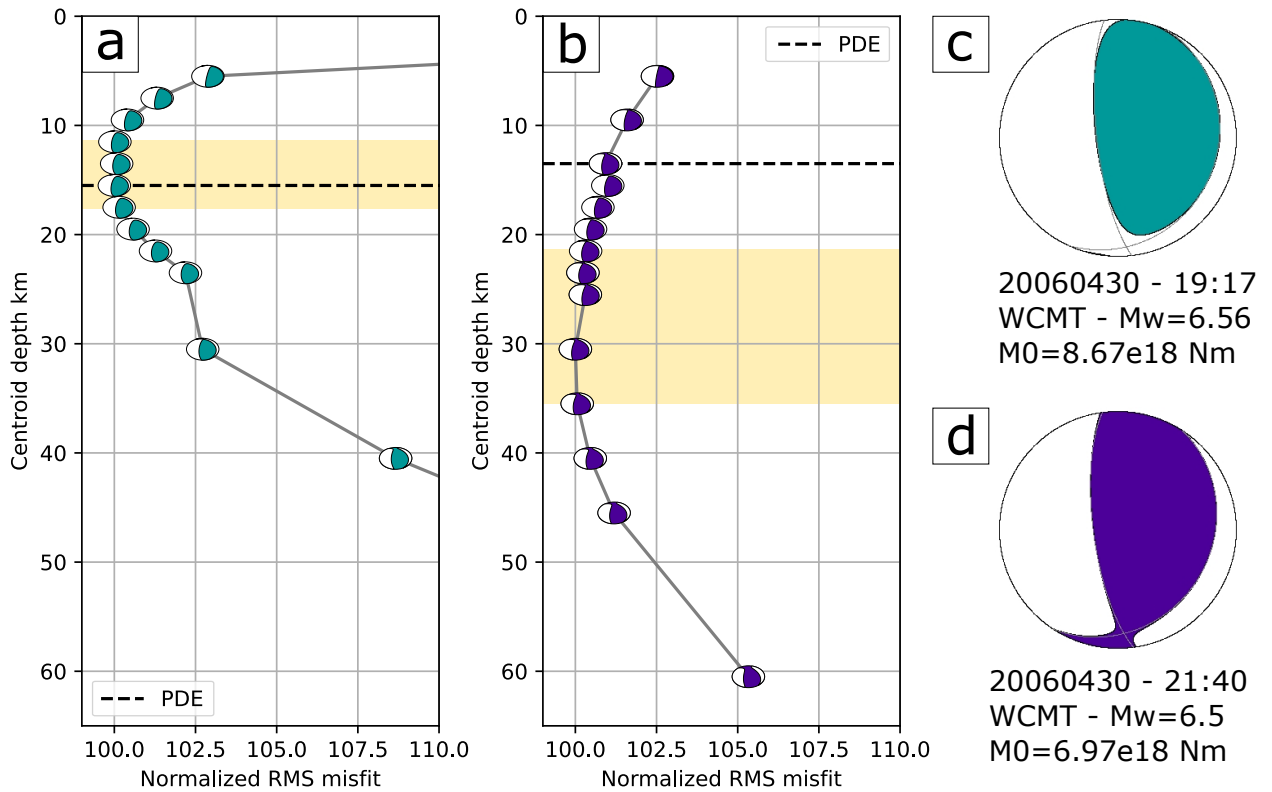


Figure 6: W-phase inversion for the 2006-04-30 19:17 (bright cyan color) and 2006-04-30 21:40 (purple color) earthquakes. Centroid depth grid search for (a) the first event and (b) the second event. The black and blue lines represent the preliminary determination of epicenter (PDE) from GCMT and optimal solutions obtained from the WCMT inversions. Preferred solutions for (c) the first earthquake and (d) the second earthquake.

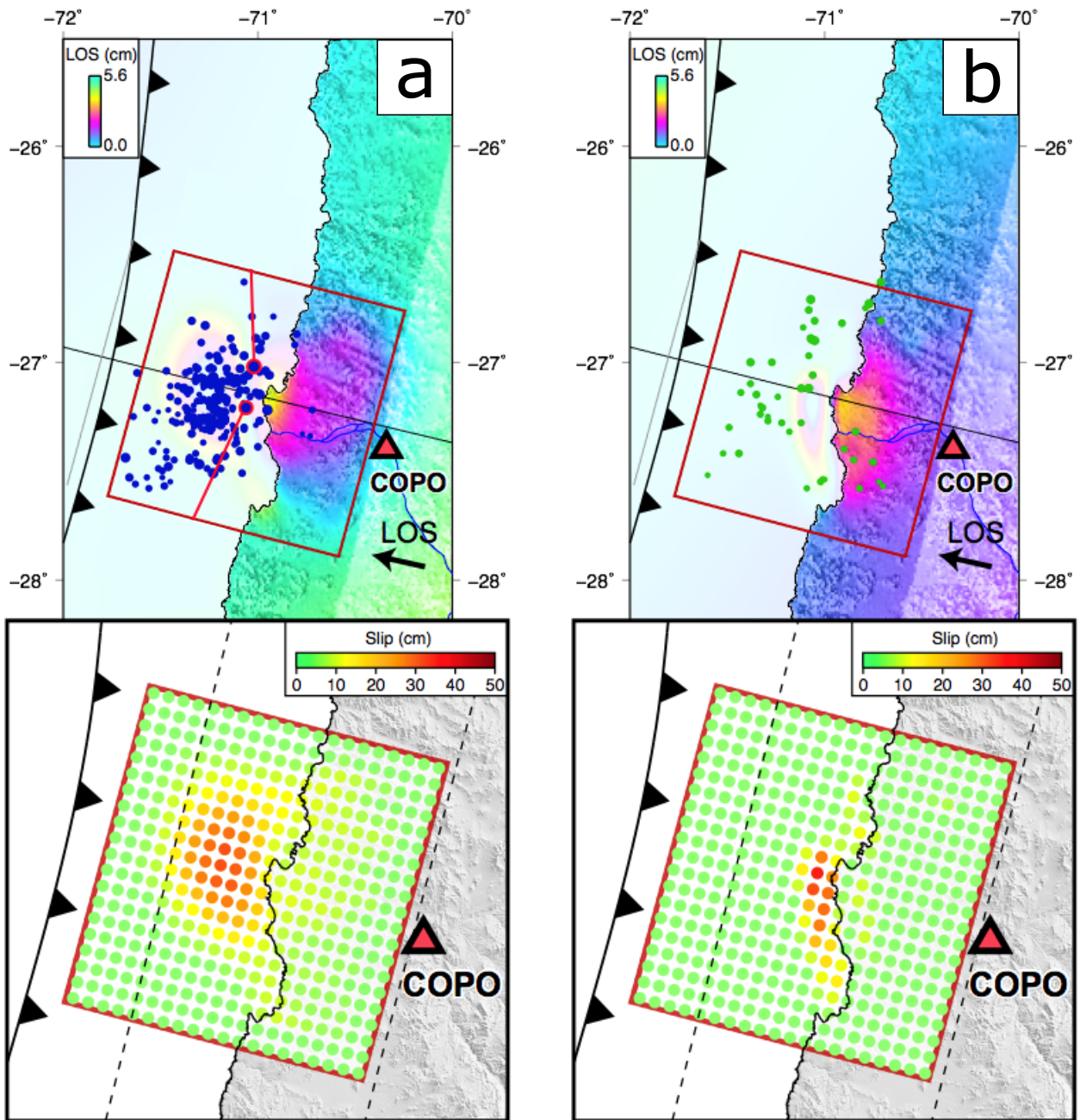


Figure 7: Surface deformation due to the 2006 Copiapó swarm determined by InSAR and the GPS station COPO. (a) Model of the “coseismic deformation” of the Copiapó swarm. The colors indicate the line-of-sight (LOS) component of the surface ground displacement derived from InSAR. The blue circles represent the seismic activity identified during the “coseismic” period between 2005-09-26 and 2006-07-03. The bottom panel shows the slip distribution model along the discretized surface fault. (b) Model of the “postseismic deformation” of the Copiapó swarm projected in LOS. The green circles represent the seismic activity identified as the aftershock during the “postseismic” period between 2006-07-03 and 2009-08-31. The bottom panel shows the postseismic slip model inverted along the discretized surface fault.

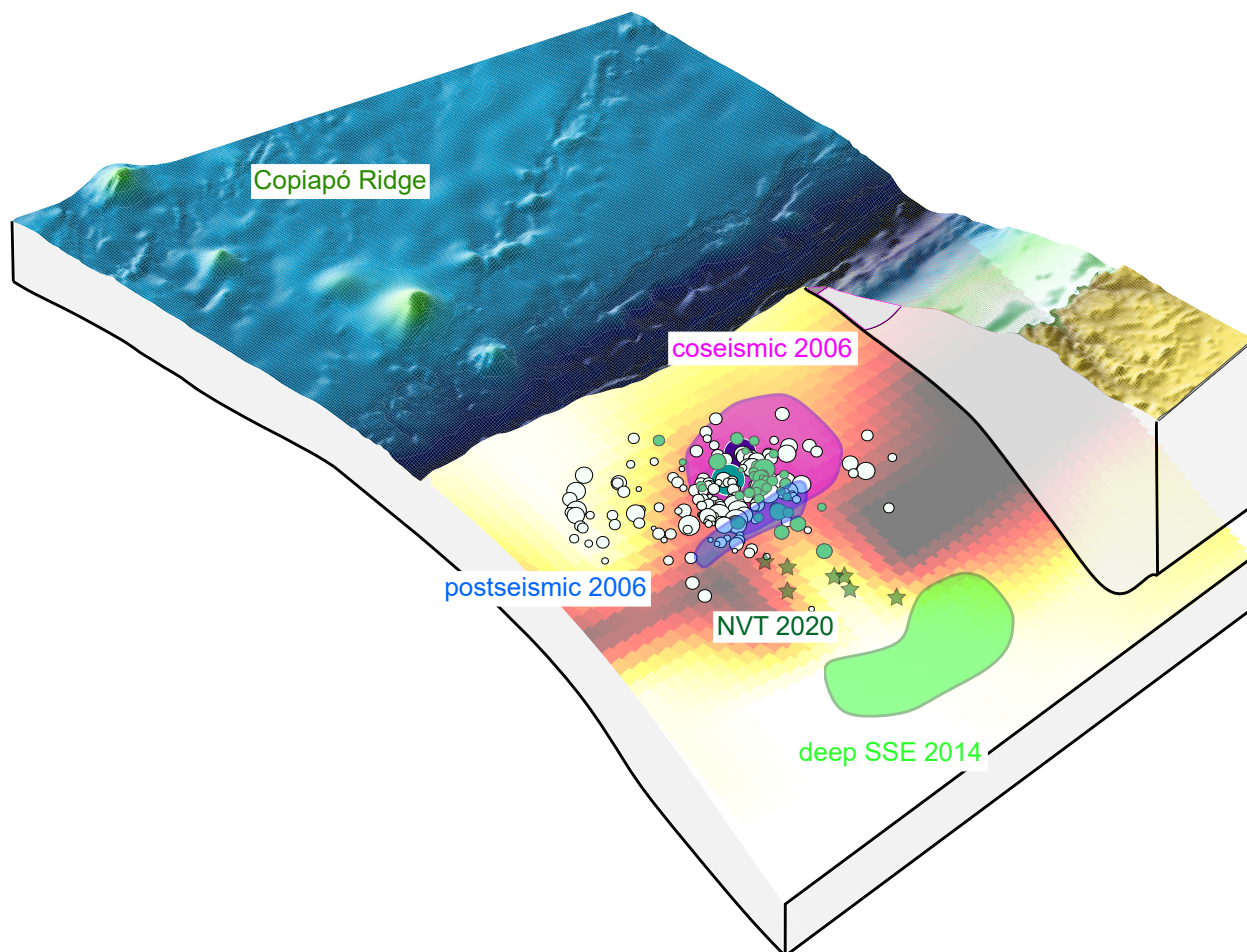


Figure 8: Schematic summary of the diversity slips behaviors observed in Copiapó. Circles represented the seismicity during April and May 2006; the green circles correspond to the seismic swarm between April 19 to April 29, while the white circles correspond to the spreading of the seismicity after the two largest earthquakes occurring on April 30 at 19:17 (bright cyan circle) and 21:40 (purple circle). The coseismic and postseismic deformation inferred from geodetic data is placed in the violet and blue areas, respectively. The star shows the location of Non-volcanic tremors (NVT) identified in 2020 (Pastén-Araya et al., 2022) and the green area corresponds to the 2014 deep SSE (Klein et al., 2018a). The red color map along the interface shows the coupling model from Klein et al. (2018b)

492 **References**

- 493 Abad, M., Izquierdo, T., Cáceres, M., Bernárdez, E., Rodríguez-Vidal, J., 2020. Coastal boulder deposit as evidence of an ocean-wide prehistoric
494 tsunami originated on the atacama desert coast (northern chile). *Sedimentology* 67, 1505–1528. doi:[doi:doi.org/10.1111/sed.12570](https://doi.org/10.1111/sed.12570).
- 495 Álvarez, O., Gimenez, M., Folguera, A., Spagnotto, S., Bustos, E., Baez, W., Braitenberg, C., 2015. New evidence about the subduction of the
496 copiapó ridge beneath south america, and its connection with the chilean-pampean flat slab, tracked by satellite geoc and egm2008 models.
497 *Journal of Geodynamics* 91, 65–88. doi:[doi:doi.org/10.1016/j.jog.2015.08.002](https://doi.org/10.1016/j.jog.2015.08.002).
- 498 Barrientos, S., 2018. The seismic network of chile. *Seismological Research Letters* 89, 467–474. doi:[doi:doi.org/10.1785/0220160195](https://doi.org/10.1785/0220160195).
- 499 Beck, S., Barrientos, S., Kausel, E., Reyes, M., 1998. Source characteristics of historic earthquakes along the central chile subduction askew et
500 alzone. *Journal of South American Earth Sciences* 11, 115–129. doi:[doi:doi.org/10.1016/S0895-9811\(98\)00005-4](https://doi.org/10.1016/S0895-9811(98)00005-4).
- 501 Bello-González, J.P., Contreras-Reyes, E., Arriagada, C., 2018. Predicted path for hotspot tracks off south america since paleocene times: Tectonic
502 implications of ridge-trench collision along the andean margin. *Gondwana Research* 64, 216–234. doi:[doi:doi.org/10.1016/j.gr.2018.07.008](https://doi.org/10.1016/j.gr.2018.07.008).
- 503 Bletery, Q., Nocquet, J.M., 2020. Slip bursts during coalescence of slow slip events in cascadia. *Nature communications* 11, 1–6. doi:[doi:doi.org/](https://doi.org/10.1038/s41467-020-15494-4)
504 [10.1038/s41467-020-15494-4](https://doi.org/10.1038/s41467-020-15494-4).
- 505 Caballero, E., Chounet, A., Duputel, Z., Jara, J., Twardzik, C., Jolivet, R., 2021. Seismic and aseismic fault slip during the initiation phase of the
506 2017 mw= 6.9 valparaíso earthquake. *Geophysical research letters* 48, e2020GL091916. doi:[doi:doi.org/10.1029/2020GL091916](https://doi.org/10.1029/2020GL091916).
- 507 Carvajal, M., Cisternas, M., Gubler, A., Catalán, P., Winckler, P., Wesson, R.L., 2017. Reexamination of the magnitudes for the 1906 and 1922
508 chilean earthquakes using japanese tsunami amplitudes: Implications for source depth constraints. *Journal of Geophysical Research: Solid Earth*
509 122, 4–17. doi:[doi:doi.org/10.1002/2016JB013269](https://doi.org/10.1002/2016JB013269).
- 510 Collot, J.Y., Sanclemente, E., Nocquet, J.M., Leprière, A., Ribodetti, A., Jarrin, P., Chlieh, M., Graindorge, D., Charvis, P., 2017. Subducted oceanic
511 relief locks the shallow megathrust in central ecuador. *Journal of Geophysical Research: Solid Earth* 122, 3286–3305. doi:[doi:doi.org/10.1002/](https://doi.org/10.1002/2016JB013849)
512 [2016JB013849](https://doi.org/10.1002/2016JB013849).
- 513 Comte, D., Haessler, H., Dorbath, L., Pardo, M., Monfret, T., Lavenu, A., Pontoise, B., Hello, Y., 2002. Seismicity and stress distribution in the
514 copiapó, northern chile subduction zone using combined on-and off-shore seismic observations. *Physics of the earth and planetary interiors* 132,
515 197–217. doi:[doi:doi.org/10.1016/S0031-9201\(02\)00052-3](https://doi.org/10.1016/S0031-9201(02)00052-3).
- 516 Comte, D., Tassara, A., Farias, M., Boroschek, R., 2006. 2006 copiapó chile seismic swarm analysis: mapping the interplate contact, in: *AGU Fall*
517 *Meeting Abstracts*, pp. S53B–1327.
- 518 Contreras-Reyes, E., Carrizo, D., 2011. Control of high oceanic features and subduction channel on earthquake ruptures along the chile–peru
519 subduction zone. *Physics of the Earth and Planetary Interiors* 186, 49–58. doi:[doi:doi.org/10.1016/j.pepi.2011.03.002](https://doi.org/10.1016/j.pepi.2011.03.002).
- 520 Das, S., Watts, A., 2009. Effect of subducting seafloor topography on the rupture characteristics of great subduction zone earthquakes, in: *Subduction*
521 *zone geodynamics*. Springer, pp. 103–118. doi:[doi:doi.org/10.1007/978-3-540-87974-9_6](https://doi.org/10.1007/978-3-540-87974-9_6).
- 522 Ducret, G., Doin, M.P., Grandin, R., Lasserre, C., Guillaso, S., 2013. Dem corrections before unwrapping in a small baseline strategy for insar time
523 series analysis. *IEEE Geoscience and Remote Sensing Letters* 11, 696–700. doi:[10.1109/LGRS.2013.2276040](https://doi.org/10.1109/LGRS.2013.2276040).
- 524 Duputel, Z., Rivera, L., 2019. The 2007 caldera collapse of Piton de la Fournaise volcano: Source process from very-long-period seismic signals.
525 *Earth Planet. Sci. Lett.* 527, 115786. doi:[10.1016/j.epsl.2019.115786](https://doi.org/10.1016/j.epsl.2019.115786).
- 526 Dziewonski, A.M., Chou, T.A., Woodhouse, J.H., 1981. Determination of earthquake source parameters from waveform data for studies of global
527 and regional seismicity. *Journal of Geophysical Research: Solid Earth* 86, 2825–2852. doi:[doi:doi.org/10.1029/JB086iB04p02825](https://doi.org/10.1029/JB086iB04p02825).
- 528 Ekström, G., Nettles, M., Dziewoński, A., 2012. The global cmt project 2004–2010: Centroid-moment tensors for 13,017 earthquakes. *Physics of*
529 *the Earth and Planetary Interiors* 200, 1–9. doi:[doi:doi.org/10.1016/j.pepi.2012.04.002](https://doi.org/10.1016/j.pepi.2012.04.002).
- 530 Grandin, R., Doin, M.P., Bollinger, L., Pinel-Puysségur, B., Ducret, G., Jolivet, R., Sapkota, S.N., 2012. Long-term growth of the himalaya inferred
531 from interseismic insar measurement. *Geology* 40, 1059–1062. doi:[doi:doi.org/10.1130/G33154.1](https://doi.org/10.1130/G33154.1).
- 532 Hayes, G.P., Moore, G.L., Portner, D.E., Hearne, M., Flamme, H., Furtney, M., Smoczyk, G.M., 2018. Slab2, a comprehensive subduction zone
533 geometry model. *Science* 362, 58–61. doi:[10.1126/science.aat4723](https://doi.org/10.1126/science.aat4723).
- 534 Holtkamp, S.G., Pritchard, M., Lohman, R., 2011. Earthquake swarms in south america. *Geophysical Journal International* 187, 128–146. doi:[doi:doi.](https://doi.org/10.1111/j.1365-246X.2011.05137.x)
535 [org/10.1111/j.1365-246X.2011.05137.x](https://doi.org/10.1111/j.1365-246X.2011.05137.x).
- 536 Hoskins, M.C., Meltzer, A., Font, Y., Agurto-Detzel, H., Vaca, S., Rolandone, F., Nocquet, J.M., Soto-Cordero, L., Stachnik, J.C., Beck, S., et al.,
537 2021. Triggered crustal earthquake swarm across subduction segment boundary after the 2016 pedernales, ecuador megathrust earthquake. *Earth*
538 *and Planetary Science Letters* 553, 116620.
- 539 Hunter, J.D., 2007. Matplotlib: A 2d graphics environment. *Computing in Science & Engineering* 9, 90–95. doi:[10.1109/MCSE.2007.55](https://doi.org/10.1109/MCSE.2007.55).

- 540 Jolivet, R., Grandin, R., Lasserre, C., Doin, M.P., Peltzer, G., 2011. Systematic insar tropospheric phase delay corrections from global meteorological
541 reanalysis data. *Geophysical Research Letters* 38. doi:doi.org/10.1029/2011GL048757.
- 542 Kanamori, H., Rivera, L., Ye, L., Lay, T., Murotani, S., Tsumura, K., 2019. New constraints on the 1922 atacama, chile, earthquake from historical
543 seismograms. *Geophysical Journal International* 219, 645–661. doi:doi.org/10.1093/gji/ggz302.
- 544 Kato, A., Fukuda, J., Kumazawa, T., Nakagawa, S., 2016. Accelerated nucleation of the 2014 iquique, chile mw 8.2 earthquake. *Scientific reports*
545 6, 1–9. doi:doi.org/10.1038/srep24792.
- 546 Klein, E., Duputel, Z., Zigone, D., Vigny, C., Boy, J.P., Doubre, C., Meneses, G., 2018a. Deep transient slow slip detected by survey gps in the
547 region of atacama, chile. *Geophysical research letters* 45, 12–263. doi:doi.org/10.1029/2018GL080613.
- 548 Klein, E., Metois, M., Meneses, G., Vigny, C., Delorme, A., 2018b. Bridging the gap between north and central chile: insight from new gps data on
549 coupling complexities and the andean sliver motion. *Geophysical Journal International* 213, 1924–1933. doi:doi.org/10.1093/gji/ggy094.
- 550 Klein, E., Potin, B., Pasten-Araya, F., Tissandier, R., Azua, K., Duputel, Z., Herrera, C., Rivera, L., Nocquet, J.M., Baez, J.C., et al., 2021.
551 Interplay of seismic and a-seismic deformation during the 2020 sequence of atacama, chile. *Earth and Planetary Science Letters* 570, 117081.
552 doi:doi.org/10.1016/j.epsl.2021.117081.
- 553 Klein, E., Vigny, C., Duputel, Z., Zigone, D., Rivera, L., Ruiz, S., Potin, B., 2022a. Return of the atacama deep slow slip event: The 5-year
554 recurrence confirmed by continuous gps. *Physics of the Earth and Planetary Interiors* doi:doi.org/10.1016/j.pepi.2022.106970.
- 555 Klein, E., Vigny, C., Nocquet, J.M., Boulze, H., 2022b. A 20 year-long gnss solution across south-america with focus in chile. *BSGF - Earth*
556 *Sciences Bulletin* doi:doi.org/10.1051/bsgf/2022005.
- 557 Krischer, L., Megies, T., Barsch, R., Beyreuther, M., Lecocq, T., Caudron, C., Wassermann, J., 2015. Obspy: A bridge for seismology into the
558 scientific python ecosystem. *Computational Science & Discovery* 8, 014003. doi:doi.org/10.1088/1749-4699/8/1/014003.
- 559 Lay, T., Kanamori, H., Ammon, C.J., Koper, K.D., Hutko, A.R., Ye, L., Yue, H., Rushing, T.M., 2012. Depth-varying rupture properties of
560 subduction zone megathrust faults. *Journal of Geophysical Research: Solid Earth* 117. doi:<https://doi.org/10.1029/2011JB009133>.
- 561 Maksymowicz, A., 2015. The geometry of the chilean continental wedge: Tectonic segmentation of subduction processes off chile. *Tectonophysics*
562 659, 183–196. doi:doi.org/10.1016/j.tecto.2015.08.007.
- 563 Manea, V.C., Leeman, W.P., Gerya, T., Manea, M., Zhu, G., 2014. Subduction of fracture zones controls mantle melting and geochemical signature
564 above slabs. *Nature communications* 5, 1–10. doi:doi.org/10.1038/ncomms6095.
- 565 Metois, M., Vigny, C., Socquet, A., 2016. Interseismic coupling, megathrust earthquakes and seismic swarms along the chilean subduction zone
566 (38–18 s). *Pure and Applied Geophysics* 173, 1431–1449. doi:doi.org/10.1007/s00024-016-1280-5.
- 567 Métois, M., Vigny, C., Socquet, A., Delorme, A., Morvan, S., Ortega, I., Valderas-Bermejo, C.M., 2014. Gps-derived interseismic coupling on the
568 subduction and seismic hazards in the atacama region, chile. *Geophysical Journal International* 196, 644–655. doi:doi.org/10.1093/gji/ggt418.
- 569
- 570 Morales-Yáñez, C., Duputel, Z., Rivera, L., 2020. Impact of 3-d earth structure on w-phase cmt parameters. *Geophysical Journal International* 223,
571 1432–1445. doi:doi.org/10.1093/gji/ggaa377.
- 572 Morell, K.D., 2016. Seamount, ridge, and transform subduction in southern central america. *Tectonics* 35, 357–385. doi:[doi.org/10.1002/](https://doi.org/10.1002/2015TC003950)
573 [2015TC003950](https://doi.org/10.1002/2015TC003950).
- 574 Nishikawa, T., Ide, S., 2015. Background seismicity rate at subduction zones linked to slab-bending-related hydration. *Geophysical Research Letters*
575 42, 7081–7089. doi:doi.org/10.1002/2015GL064578.
- 576 Nishikawa, T., Ide, S., 2017. Detection of earthquake swarms at subduction zones globally: Insights into tectonic controls on swarm activity. *Journal*
577 *of Geophysical Research: Solid Earth* 122, 5325–5343. doi:<https://doi.org/10.1002/2017JB014188>.
- 578 Okada, Y., 1985. Surface deformation due to shear and tensile faults in a half-space. *Bulletin of the seismological society of America* 75, 1135–1154.
579 doi:doi.org/10.1785/BSSA0750041135.
- 580 Pastén-Araya, F., Potin, B., Azua, K., Saez, M., Aden-Antoniów, F., Ruiz, S., Cabrera, L., Ampuero, J.P., Nocquet, J.M., Rivera, L., et al., 2022.
581 Along-dip segmentation of the slip behavior and rheology of the copiapó ridge subducted in north-central chile. *Geophysical Research Letters*
582 49, e2021GL095471. doi:doi.org/10.1029/2021GL095471.
- 583 Peacock, S.A., 1990. Fluid processes in subduction zones. *Science* 248, 329–337. doi:[10.1126/science.248.4953.329](https://doi.org/10.1126/science.248.4953.329).
- 584 Poli, P., Maksymowicz, A., Ruiz, S., 2017. The mw 8.3 illapel earthquake (chile): Preseismic and postseismic activity associated with hydrated
585 slab structures. *Geology* 45, 247–250. doi:doi.org/10.1130/G38522.1.
- 586 Radiguet, M., Cotton, F., Vergnolle, M., Campillo, M., Walpersdorf, A., Cotte, N., Kostoglodov, V., 2012. Slow slip events and strain accumulation
587 in the guerrero gap, mexico. *Journal of Geophysical Research: Solid Earth* 117. doi:doi.org/10.1029/2011JB008801.
- 588 Ruiz, J.A., Contreras-Reyes, E., Ortega-Culaciati, F., Manríquez, P., 2018. Rupture process of the april 24, 2017, mw 6.9 valparaíso earthquake

- 589 from the joint inversion of teleseismic body waves and near-field data. *Physics of the Earth and Planetary Interiors* 279, 1–14. doi:doi.org/10.1016/j.pepi.2018.03.007.
- 590
- 591 Ruiz, S., Aden-Antoniow, F., Baez, J., Otarola, C., Potin, B., Del Campo, F., Poli, P., Flores, C., Satriano, C., Leyton, F., et al., 2017. Nucleation
592 phase and dynamic inversion of the mw 6.9 valparaíso 2017 earthquake in central chile. *Geophysical Research Letters* 44, 10–290. doi:doi.org/10.1002/2017GL075675.
- 593
- 594 Ruiz, S., Grandin, R., Dionicio, V., Satriano, C., Fuenzalida, A., Vigny, C., Kiraly, E., Meyer, C., Baez, J.C., Riquelme, S., et al., 2013. The
595 constitución earthquake of 25 march 2012: a large aftershock of the maule earthquake near the bottom of the seismogenic zone. *Earth and
596 Planetary Science Letters* 377, 347–357. doi:doi.org/10.1016/j.epsl.2013.07.017.
- 597 Ruiz, S., Madariaga, R., 2018. Historical and recent large megathrust earthquakes in chile. *Tectonophysics* 733, 37–56. doi:[doi.org/10.1016/](https://doi.org/10.1016/j.tecto.2018.01.015)
598 [j.tecto.2018.01.015](https://doi.org/10.1016/j.tecto.2018.01.015).
- 599 Ruiz, S., Metois, M., Fuenzalida, A., Ruiz, J., Leyton, F., Grandin, R., Vigny, C., Madariaga, R., Campos, J., 2014. Intense foreshocks and a slow
600 slip event preceded the 2014 iquique m w 8.1 earthquake. *Science* 345, 1165–1169. doi:[10.1126/science.1256074](https://doi.org/10.1126/science.1256074).
- 601 Salazar, D., Easton, G., Goff, J., Guendon, J.L., González-Alfaro, J., Andrade, P., Villagrán, X., Fuentes, M., León, T., Abad, M., et al., 2022. Did
602 a 3800-year-old m w 9.5 earthquake trigger major social disruption in the atacama desert? *Science advances* 8, eabm2996. doi:[10.1126/](https://doi.org/10.1126/sciadv.abm2996)
603 [sciadv.abm2996](https://doi.org/10.1126/sciadv.abm2996).
- 604 Segovia, M., Font, Y., Régnier, M., Charvis, P., Galve, A., Nocquet, J.M., Jarrín, P., Hello, Y., Ruiz, M., Pazmiño, A., 2018. Seismicity distribution
605 near a subducting seamount in the central ecuadorian subduction zone, space-time relation to a slow-slip event. *Tectonics* 37, 2106–2123.
606 doi:doi.org/10.1029/2017TC004771.
- 607 Shapiro, S., Patzig, R., Rothert, E., Rindschwentner, J., 2003. Triggering of seismicity by pore-pressure perturbations: Permeability-related signa-
608 tures of the phenomenon, in: *Thermo-Hydro-Mechanical Coupling in Fractured Rock*. Springer, pp. 1051–1066.
- 609 Shapiro, S.A., Huenges, E., Borm, G., 1997. Estimating the crust permeability from fluid-injection-induced seismic emission at the ktb site.
610 *Geophysical Journal International* 131, F15–F18. doi:doi.org/10.1111/j.1365-246X.1997.tb01215.x.
- 611 Shelly, D.R., Beroza, G.C., Ide, S., 2007. Complex evolution of transient slip derived from precise tremor locations in western shikoku, japan.
612 *Geochemistry, Geophysics, Geosystems* 8. doi:doi.org/10.1029/2007GC001640.
- 613 Singh, S.C., Hananto, N., Mukti, M., Robinson, D.P., Das, S., Chauhan, A., Carton, H., Gratacos, B., Midnet, S., Djajadihardja, Y., et al., 2011.
614 Aseismic zone and earthquake segmentation associated with a deep subducted seamount in sumatra. *Nature Geoscience* 4, 308–311. doi:doi.org/10.1038/ngeo1119.
- 615
- 616 Tissandier, R., Nocquet, J., Klein, E., Vigny, C., Ojeda, J., Ruiz, S., 2023. Afterslip of the mw 8.3 2015 illapel earthquake imaged through a time-
617 dependent inversion of continuous and survey gnss data. *Journal of Geophysical Research: Solid Earth* 128. doi:[10.1029/2022jb024778](https://doi.org/10.1029/2022jb024778).
- 618 Uchida, N., 2019. Detection of repeating earthquakes and their application in characterizing slow fault slip. *Progress in Earth and Planetary Science*
619 6. doi:[10.1186/s40645-019-0284-z](https://doi.org/10.1186/s40645-019-0284-z).
- 620 Uchida, N., Bürgmann, R., 2019. Repeating earthquakes. *Annual Review of Earth and Planetary Sciences* 47, 305–332. doi:[10.1146/](https://doi.org/10.1146/annurev-earth-053018-060119)
621 [annurev-earth-053018-060119](https://doi.org/10.1146/annurev-earth-053018-060119).
- 622 Uieda, L., Tian, D., Leong, W.J., Schlitzer, W., Toney, L., Grund, M., Jones, M., Yao, J., Materna, K., Newton, T., Anant, A., Ziebarth, M., Wessel,
623 P., 2021. Pygmt: A python interface for the generic mapping tools. doi:[10.5281/zenodo.4978645](https://doi.org/10.5281/zenodo.4978645).
- 624 Vaca, S., Vallée, M., Nocquet, J.M., Battaglia, J., Régnier, M., 2018. Recurrent slow slip events as a barrier to the northward rupture propagation
625 of the 2016 pedernales earthquake (central ecuador). *Tectonophysics* 724, 80–92. doi:doi.org/10.1016/j.tecto.2017.12.012.
- 626 Valenzuela-Malebrán, C., Cesca, S., Ruiz, S., Passarelli, L., Leyton, F., Hainzl, S., Potin, B., Dahm, T., 2021. Seismicity clusters in central
627 chile: investigating the role of repeating earthquakes and swarms in a subduction region. *Geophysical Journal International* 224, 2028–2043.
628 doi:doi.org/10.1093/gji/ggaa562.
- 629 Vallée, M., Nocquet, J.M., Battaglia, J., Font, Y., Segovia, M., Regnier, M., Mothes, P., Jarrin, P., Cisneros, D., Vaca, S., et al., 2013. Intense
630 interface seismicity triggered by a shallow slow slip event in the central ecuador subduction zone. *Journal of Geophysical Research: Solid Earth*
631 118, 2965–2981. doi:doi.org/10.1002/jgrb.50216.
- 632 Vigny, C., Rudloff, A., Ruegg, J.C., Madariaga, R., Campos, J., Alvarez, M., 2009. Upper plate deformation measured by gps in the coquimbo gap,
633 chile. *Physics of the Earth and Planetary Interiors* 175, 86–95. doi:doi.org/10.1016/j.pepi.2008.02.013.
- 634 Villegas-Lanza, J.C., Nocquet, J.M., Rolandone, F., Vallée, M., Tavera, H., Bondoux, F., Tran, T., Martin, X., Chlieh, M., 2016. A mixed seismic-
635 aseismic stress release episode in the andean subduction zone. *Nature Geoscience* 9, 150–154. doi:doi.org/10.1038/ngeo2620.
- 636 Wallace, L.M., Beavan, J., Bannister, S., Williams, C., 2012. Simultaneous long-term and short-term slow slip events at the hikurangi subduction
637 margin, new zealand: Implications for processes that control slow slip event occurrence, duration, and migration. *Journal of Geophysical*

- 638 Research: Solid Earth 117. doi:doi.org/10.1029/2012JB009489.
- 639 Wang, K., Bilek, S.L., 2011. Do subducting seamounts generate or stop large earthquakes? *Geology* 39, 819–822. doi:[doi.org/10.1130/](https://doi.org/10.1130/G31856.1)
- 640 [G31856.1](https://doi.org/10.1130/G31856.1).
- 641 Wang, K., Bilek, S.L., 2014. Fault creep caused by subduction of rough seafloor relief. *Tectonophysics* 610, 1–24. doi:[doi.org/10.1016/j.](https://doi.org/10.1016/j.tecto.2013.11.024)
- 642 [tecto.2013.11.024](https://doi.org/10.1016/j.tecto.2013.11.024).